THERMODYNAMICS AND APPLICATIONS OF ELASTIN-LIKE POLYPEPTIDES

A Dissertation

by

YOUN HEE CHO

Submitted to the Office of Graduate Studies of
Texas A&M University
in partial fulfillment of the requirements for the degree of

DOCTOR OF PHILOSOPHY

August 2009

Major Subject: Chemistry

THERMODYNAMICS AND APPLICATIONS OF ELASTIN-LIKE POLYPEPTIDES

A Dissertation

by

YOUN HEE CHO

Submitted to the Office of Graduate Studies of
Texas A&M University
in partial fulfillment of the requirements for the degree of

DOCTOR OF PHILOSOPHY

Approved by:

Chair of Committee,	Paul S. Cremer
Committee Members,	J. Martin Scholtz
	David E. Bergbreiter
	D. Wayne Goodman
Head of Department,	David H. Russell

August 2009

Major Subject: Chemistry

ABSTRACT

Thermodynamics and Applications of Elastin-like Polypeptides. (August 2009)

Youn Hee Cho, B.S., State University of New York at Purchase

Chair of Advisory Committee: Dr. Paul S. Cremer

Understanding protein stability and folding is of central importance in chemistry, biology, and medicine. Despite its importance, a molecular level understanding of protein stability still remains illusive due to the complexity of the system. In this study, we employed protein-like polypeptides to study several aspects of protein stability in different aqueous environments. The model system employed here is elastin-like polypeptides (ELPs).

First, the modulation of the lower critical solution temperature (LCST) of neutral ELPs was investigated in the presence of 11 sodium salts that span the Hofmeister series for anions. It was found that the hydrophobic collapse/aggregation of these ELPs generally followed the series. Specifically, kosmotropic anions decreased the LCST by polarizing interfacial water molecules involved in hydrating amide groups on the ELPs. By contrast, chaotropic anions lowered the LCST through a surface tension effect. Additionally, chaotropic anions showed salting-in properties at low salt concentrations that were related to the saturation binding of anions with the biopolymers. These overall mechanistic effects were also compared to the results previously found for the hydrophobic collapse and aggregation of poly(*N*-isoproplyacrylamide). A positively

charged ELP, ELP KV_6-112, was used as a next model system. We observed both inverse and direct Hofmeister effects on LCST with five chaotropic salts.

Next, the solvent isotope effects on the LCST of ELPs were investigated as a function of ELP chain length and guest residue chemistry using D_2O and H_2O. Differences in the LCST values with heavy and light water were correlated with secondary structure formation of the polypeptide chains which was quantified by circular dichroism, FTIR, and differential scanning calorimetry measurements. It was found that there is a great change in the LCST values between H_2O and D_2O for those polypeptides which form the greatest amount of β-spiral structure. This study suggests that hydrogen bonding rather than hydrophobicity is the key factor in the stabilization of ELPs in D_2O over H_2O.

The phase transition property of ELPs can also be applied to development of stimuli responsive biosensor system. In this study, we employed ELP-conjugate solid supported lipid bilayer as a size selective binding sensor.

DEDICATION

To my parents, Sung-Kook Cho and Youn-Hwa Park

ACKNOWLEDGEMENTS

First, I would like to thank my advisor Prof. Paul S. Cremer for his support and encouragements throughout the Ph.D. program. I also thank my committee members, Prof. J. Martin Scholtz, Prof. David E. Bergbreiter, and Prof. D. Wayne Goodman, for their help and support.

Thanks also go to my friends and colleagues at Texas A&M University, Dr. Soonmi Lim, Marcus, Srinivas, Soyoun, Panida, Veronica, Dr. Yanjie Zhang, Dr. Laura B. Sagle, Dr. Katherine Cimatu, Jaibir Kherb, Jennifer Jones, Dr. Tinglu Yang, Dr. Jinjun Shi, Dr. Arnaldo Diaz, Dr. Weissu Liao, Dr. Hyunsook Jung, and the department faculty and staff, for making my time at Texas A&M University a great experience.

Finally, thanks to my parents, sister, and my boyfriend Ed for their support, patience, and love.

TABLE OF CONTENTS

CHAPTER Page

LIST OF FIGURES

FIGURE Page

FIGURE Page

FIGURE Page

LIST OF TABLES

CHAPTER I

INTRODUCTION

Hofmeister Series

Inorganic salts have a strong effect on protein solubility. For this reason, salt–induced protein precipitation is frequently used in protein purification proceeses.[1] The solubility of proteins in different salt solutions typically follows a recurring trend, known as the Hofmeister series.[2] The effects associated with this trend are typically more pronounced for anions than cations. The anion series is as follows:

$$CO_3^{2-} > SO_4^{2-} > S_2O_3^{2-} > H_2PO_4^- > F^- > Cl^- > Br^- \sim NO_3^- > I^- > ClO_4^- > SCN^-$$

The anions can be categorized into two general groups based upon the physical behavior of aqueous-macromolecular systems in their presence. Specifically, species to the left of Cl^- are called kosmotropes and have been shown to salt protein molecules out of solution. On the other hand, species to the right of Cl^- are called chaotropes and are known to increase the solubility of protein molecules in solution.[3]

Since it was first discovered 120 years ago, the Hofmeister series has been found to apply to a plethora of biological and chemical phenomena in addition to protein precipitation. These include protein crystallization, enzyme turnover rates, and micelle formation.[4] Despite its wide use, a molecular level understanding of this series has remained elusive for over a century.[5-7]

This dissertation follows the style of *Journal of the American Chemical Society.*

Recently, it has been shown that the ability of a particular salt to affect the structure of water in bulk solution probably plays little, if any, role in the Hofmeister effect.[5-9] For example, Bakker and coworkers reported that the presence of SO_4^{2-} or ClO_4^- ions do not effect the hydrogen bonding network of water beyond the first hydration shell.[7] Pielak and coworkers demonstrated that the solute's impact on water structure is not correlated to its effect on protein stability.[5] Furthermore, our laboratory has shown that water molecules adjacent to a Langmuir monolayer do not necessarily show structural variations consistent with this series even when the physical properties of the monolayer itself strictly follow the series.[6] Most recently, Saykally and Geissler have investigated the Raman spectra of aqueous salt solutions. Their work also shows little evidence of bulk water structure making and breaking effects for the ions.[8]

In contrast to the role of ions on water structure, it has been demonstrated that direct interactions between ions and macromolecules can be key to understanding the Hofmeister series.[10-13] (Figure 1.1)

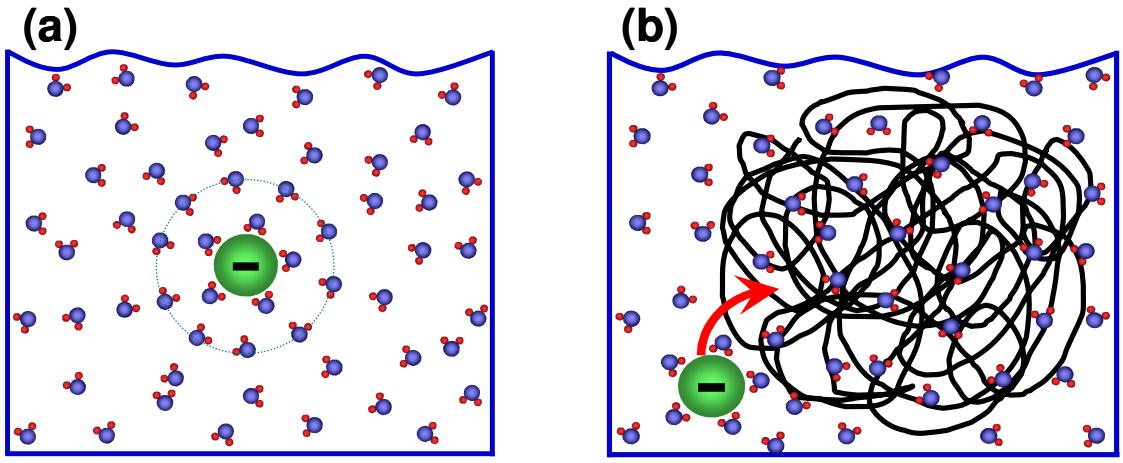

Figure 1.1. Schematic diagram of indirect and direct anion effects. (a) anions effects to order the water beyond its first hydration shell is needed for a bulk water effects. (b) direct interaction of anions with biomacromolecules in aqueous solution.

In fact, proposed mechanisms to explain the physical properties of macromolecules in solution have involved dispersion forces, ion binding to the macromolecules, as well as the modulation of surface tension by the ions.[10-12,14,15] Recently, our laboratory has reported the effects of Hofmeister anions on the lower critical solution temperature (LCST) of poly (*N*-isoproplyacrylamide), PNIPAM. This work, which studied the effects of 11 different anions, showed that changes in the LCST of PNIPAM were caused by completely different mechanisms for chaotropes and kosmotropes.[16] Specifically, chaotropic anions depressed the LCST by increasing the surface tension at the polymer/water interface at higher salt concentrations. At lower concentrations, they also increased the LCST through a direct anion binding mechanism that followed a Langmuir isotherm. On the other hand, kosmotropic anions generally depressed the LCST of the polymer by polarizing interfacial water molecules. This polarization effect weakened the hydrogen bonding of water to a molecule's carbonyl groups.

PNIPAM consists of monomers that are isomers of isoleucine and its LCST is thought to be a good mimic for the cold denaturation of proteins.[17] The key difference between this polymer and a polypeptide is that the amide moiety is pendent rather than part of the backbone (Figure 1.2). Therefore, it is important to determine whether the mechanism that governs the modulation of the LCST of PNIPAM as salts are added to solution can be extended to the much more important case of polypeptides. To this end, we have employed elastin-like polypeptides (ELPs) as a model polypeptide system, which also exhibits LCST phase behavior.

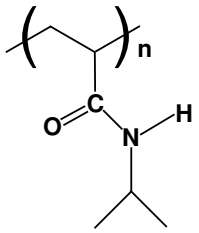

Figure 1.2. Structure of PNIPAM.

Elastin-like Polypeptides

We chose ELPs as a model for more complex protein constructs. Like proteins, ELPs are composed of amino acids so that the sequence and chain length of ELPs can be precisely controlled by recombinant synthesis.[18,19] Unlike proteins, however, which typically have nonrepetitive sequences and well-defined tertiary structures, ELPs are considerably simpler repetitive polypeptides that consist of a five residue repeat, VPGXG, whereby X can be any amino acid except proline. Therefore, ELPs provide a simple but powerful polypeptide model to carry out systematic structure-property studies of polypeptides in solution. Significant sequence diversity can be achieved by substituting various amino acids at the fourth position.

Like PNIPAM, ELPs precipitate from solutions above their LCST value.[20,21] However, PNIPAM undergoes hydrophobic collapse/aggregation without the formation of specific secondary or tertiary structures. On the other hand, the collapse and aggregation of ELPs is associated with significant β–turn/β-spiral secondary/tertiary structure formation.[22] Such properties afford an interesting bridge between the purely LCST driven behavior of PNIPAM and the more complex folding and cold denaturation behavior exhibited by typical proteins

Temperature Gradient Devices

The temperature-gradient apparatus consisted of two brass tubes (1/8 in wide, K&S Engineering, Chicago, IL) placed parallel to each other. A hot solution was flowed inside one tube while a cold solution was flowed inside the other to create a linear temperature gradient over a 5 mm gap between them.[23] A cover glass was placed over the

brass tubes as a sample stage. ELP solutions were placed inside rectangular borosilicate capillary tubes (VitroCom, Inc.) with dimensions of 2 cm × 1 mm × 100 μm (length × width × height). Six tubes were placed on the sample stage with their long axis parallel to the temperature gradient. (Figure 1.3) In each case, 4 capillaries contained samples while the other two tubes contained standards with known LCST values to calibrate the temperature gradient.

In a typical experiment, six capillary tubes were placed side-by-side and imaged by dark field microscopy with a 2X objective under an inverted microscope (TE2000-U, Nikon). Light scattering images from the capillary tubes were captured with a CCD camera (Micromax 1024, Princeton Instruments) using dark field optics. The LCST of the ELPs and PNIPAM were measured as an abrupt change in the amount of light scattering found in a dark field image.[16,24,25]

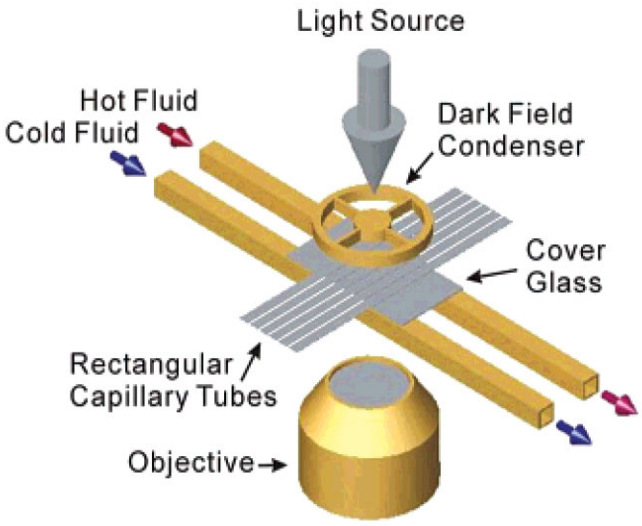

Figure 1.3. Schematic diagram of temperature gradient device.

CHAPTER II

SPECIFIC ANION EFFECTS ON PHASE TRANSTION TEMPERATURES OF NEUTRAL ELASTIN-LIKE POLYPEPTIDES

Introduction

Herein, Hofmeister effects were investigated for two different ELPs using 11 different sodium salts. The ELPs employed were ELP V_5-120 and ELP $V_5A_2G_3$-120. Both molecules consist of 120 repeats of the VPGXG sequence. However, the first molecule has V at all guest residue positions, while the second, more hydrophilic ELP contains a mixture of V, A, and G guest residues in a 5:2:3 ratio. The results of the present ELP studies showed a general correlation with data from PNIPAM,[16] although several key differences were also found.

The overall mechanism for the modulation of the LCST is presented in Figure 2.1. As shown, the kosmotropic anions weaken the hydrogen bonding of water to the carbonyl moiety of the amide backbone (Figure 2.1a). This effect is manifest by a strong correlation between the change in the LCST of the ELP and the entropy of hydration values for the kosmotropes. By contrast, chaotropes depress the LCST values by weakening the hydrophobic hydration of the biomacromolecule (Figure 2.1b). Evidence for this effect comes from a strong correlation between the LCST of the biopolymers and the surface tension increment values,σ for the anions. Concomitantly with salting-out effects, there is also a salting-in effect caused by direct binding of chaotropic anions with the amide moieties (Figure 2.1c). This direct ion binding effect shows Langmuir isotherm type behavior. It should be noted that the effects described in Figure 2.1 a&b

were found to be correlated with a linear decrease in the LCST of the ELPs per mole of added salt, while the effect shown in Figure 2.1c was associated with an increase in the LCST and was a saturation effect.

Experimental

ELP Preparation

The pET plasmids employed herein were constructed using recursive directional ligation as previously described.[18] The plasmids were expressed in BLR/DE3 *E. coli* in high growth media (TBdry) supplemented with ampicillin. Expression was carried out for 24 hours without isopropyl-β-D-thio-galactoside induction and resulted in typical yields of 200-300 mg per liter of cell culture medium. Purification of the ELP was done via sonication of the cells followed by a series of inverse transition cycling (ITC) steps. For example, one round of ITC was carried out by centrifugation at 10,000 g at 50 ºC by adding 1 M NaCl. The pellets (containing ELP) were then dissolved in phosphate buffer (10 mM, pH 6.9, 4 ºC) and the remaining cellular debris was removed by centrifugation at 10,000 g. Typically, two rounds of ITC were needed to remove impurities. The molecular weight and purity of the ELPs were assessed by SDS-PAGE and $CuCl_2$-staining. The concentrations of the purified ELP solutions were determined by measuring the absorbance at 280 nm (ε =5690 M^{-1} cm^{-1}). After purification by ITC, samples were dialyzed against purified water (NANOpure Ultrapure Water System, Barnstead, Dubuque, IA) with a minimum resistivity of 18 MΩ·cm to remove residual salts. Finally, the samples were lyophilized and stored at -80 ºC until use.

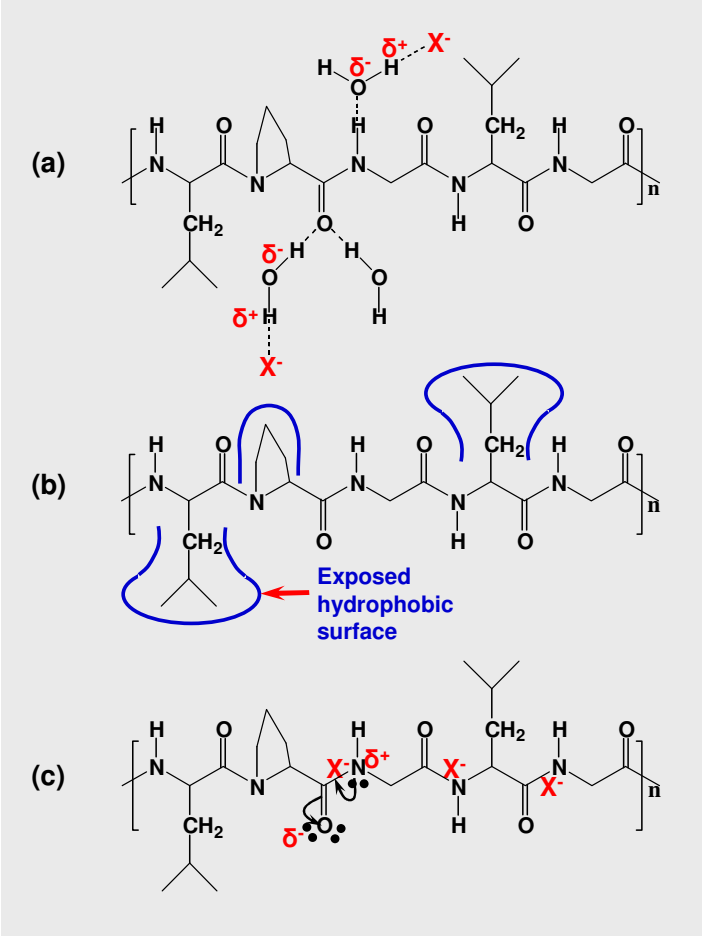

Figure 2.1. Proposed mechanisms for specific anion effects on the LCST of ELP V_5-120. (a) Direct interactions of anions with water involved in hydrogen bonding to the amide. Kosmotropic anions polarize these water molecules and thereby weaken the hydrogen bonding of water to the macromolecule, a salting-out effect. (b) The blue lines represent the hydrophobically hydrated regions of the biomacromolecule. The cost of such hydration increases as salt is added to solution. (c) Direct ion binding of chaotropic anions to the amide moieties along the backbone of the polypeptide should cause a salting-in effect.

LCST Measurements

NaSCN, NaI, $NaClO_4$, NaBr, $NaNO_3$, NaCl, NaF, NaH_2PO_4, $Na_2S_2O_3$, Na_2SO_4, and Na_2CO_3were purchased from Sigma Aldrich (>99% purity). The salts were dissolved in 10 mM phosphate buffer (pH 6.9) made with purified water from the NANOpure Ultrapure Water System. ELPs were dissolved in salt solutions at a polypeptide concentration of 6.4 mg/mL. The LCST values of the ELP solutions were measured using a microfluidic temperature-gradient apparatus placed under a dark field microscope.[24] The standard solutions were 10 mg/mL PNIPAM in water without salt and 10 mg/mL PNIPAM in 0.35M KCl, which had LCST values of 30.9 ºC and 22.7 ºC, respectively. For high temperature measurements (above 40 ºC) two organic standards, octadecanol and 1, 2- decanethiol, were used. The melting temperatures of the organic samples were determined independently in a melting temperature apparatus (Optimelt MPA100, Stanford Research System) and had values of 58.5 ± 0.3 for octadecanol and 46.1 ± 0.2 for 1, 2- decanethiol.

It should be noted that there is a sharp increase in the amount of light scattered at temperatures above which the polypeptides undergo hydrophobic collapse/aggregation. On the other hand, the organic samples scattered significantly more light in the solid state than above their melting point. The temperature along the long axis of the tube was assumed to vary linearly as a function of distance as has been previously shown.[23] Metamorph software (Universal Imaging Corp.) was used to create line profiles of light scattering as a function of position. These line profiles were used to abstract the exact

phase transition temperatures following our standard procedures. All LCST values reported herein represent an average of eight measurements.

Results

LCST of ELP V_5-120 with Hofmeister Salts

Six glass capillaries containing sample solutions are placed parallel to the temperature gradient on the sample stage of a dark field microscopy. As the temperature increases linearly from left to the right in Figure 2.2, solution gets cloudy at different position indicating the differences in phase transition of the sample. Very top and bottom capillaries contain PNIPAM standard with a known LCST values. The pixel positions of these two standards are used to convert the pixel to temperature. A straight line is drawn across the clear/cloudy region of the each capillary in order to determine the accurate phase transition point. Line scan profile (Figure 2.3) of each sample is generated and the onset point of the profile is taken as LCST value.

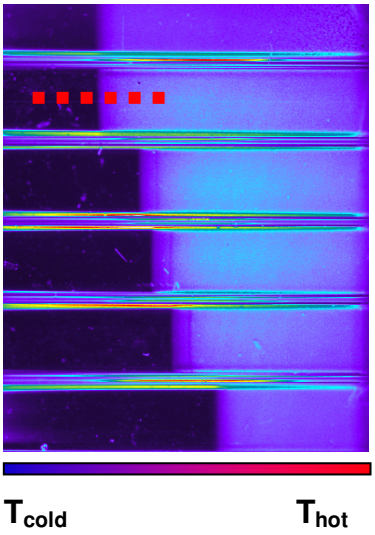

Figure 2.2. Dark filed microscopy image of 6.4 mg/ml ELP V-120 phase transition. From top to bottom of the image: PNIPAM in 0.35 KCl, ELP V-120 in 0.4 M NaCl, ELP V-120 in 0.2 M NaCl, ELP V-120 in 0.1 M NaCl, ELP V-120 in 0 M NaCl, and PNIPAM in H_2O. Red dotted line is a line scan across the phase transition region of the sample.

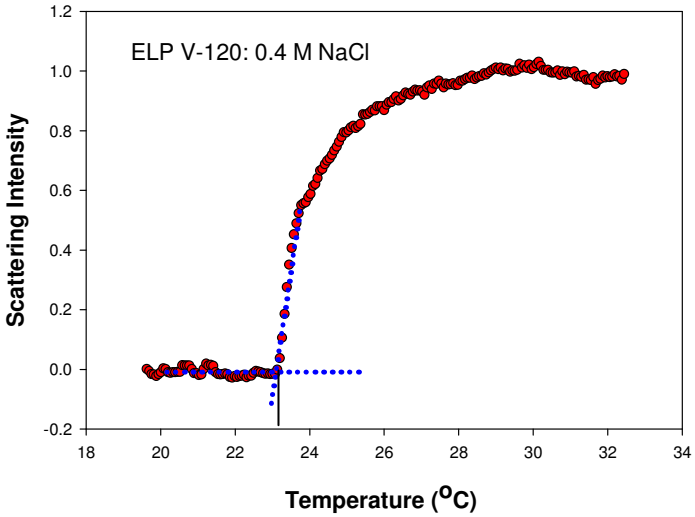

Figure 2.3. Line scan profile of the red dotted region in Fig. 2.2. The onset point of the phase transition curve is taken as the LCST value.

In a first set of experiments, the LCST values of ELP V_5-120 were determined as a function of salt type and concentration for the 11 sodium salts investigated (Figure 2.4). The phase transition occurs at ~28 ºC in the absence of salt. Moreover, the kosmotropic anions, F^-, $H_2PO_4^-$, $S_2O_3^{2-}$, SO_4^{2-}, CO_3^{2-} as well as Cl^- display linear salting-out behavior. The data from these anions can be fit by a simple linear equation (eqn. 2.1):

$$T = T_0 + c[\mathrm{M}] \tag{2.1}$$

whereby T_0 is the LCST value in the absence of salt. The term c is a constant with units of temperature/molarity, and [M] is the molar concentration of salt. The c values for these kosmotropes are reported on page 31 in Table 2.1.

In contrast with the kosmotropes, the chaotropic anions (SCN^-, I^-, ClO_4^-, Br^-, NO_3^-) show non-linear changes in their LCST values as a function of added salt. In fact, the LCST values for SCN^- and I^- actually increase at low salt concentration before salting out behavior becomes dominant at higher salt concentration. The shape of these curves can be well fit by adding a binding isotherm to the linear term used for the kosmotropes (eqn. 2.2):

$$T = T_0 + c[\mathrm{M}] + \frac{B_{\max} K_A[M]}{1 + K_A[M]} \tag{2.2}$$

The first two terms in eqn. 2.2 have the same meanings as in eqn. 2.1. The last term is a Langmuir binding isotherm, where K_A is the apparent equilibrium association constant. Since the isotherm is unitless, a constant, B_{max}, is added, which has units of temperature. This constant is interpreted as the increase in the LCST value found when a saturation

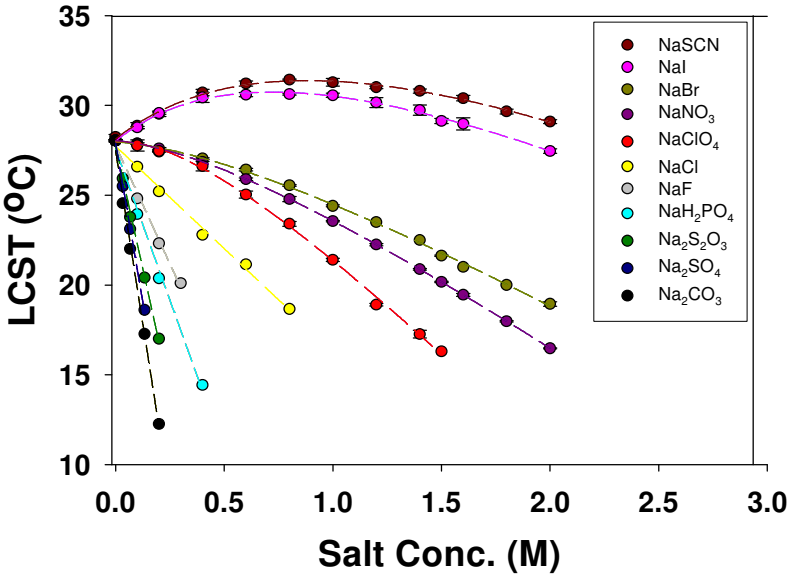

Figure 2.4. LCST vs. salt concentration curves for a series of sodium salts with ELP V_5-120. Each data point represents the average of 8 measurements and the standard deviations are within the size of the circular data points in all cases. The dashed lines are fits to the data using eqns. 1&2.

concentration of salt is present. The B_{max}, K_A, and c values determined with the chaotropic anions are reported on page 35 in Table 2.1. The c values for ELP V_5-120 in the presence of the 11 sodium salts are plotted against the known entropy of hydration values, ΔS_{hydr},[26] for each of the anions employed (Figure 2.5a). As can be seen, the correlation between c and ΔS_{hydr} is excellent for the kosmotropes, but not for the chaotropes. Changing the x-axis to the surface tension increment, σ for each of the anions shows excellent correlation to the chaotropes, but the kosmotropes are uncorrelated (Figure 2.5b). It should be noted that the surface tension increment refers to the measured change in surface tension at the air/water interface per mole of salt added to the solution. It should be further noted that the c values were also tested against other thermodynamic parameters such as polarizability, ionic volume, and viscosity coefficient; however, the data were uncorrelated. Significantly, the trends found here were identical to the ones previously found for the LCST of PNIPAM.[16] Namely, the entropies of hydration were correlated with the c values of the kosmotropes, while the surface tension increments were correlated with the c values of the chaotropes.

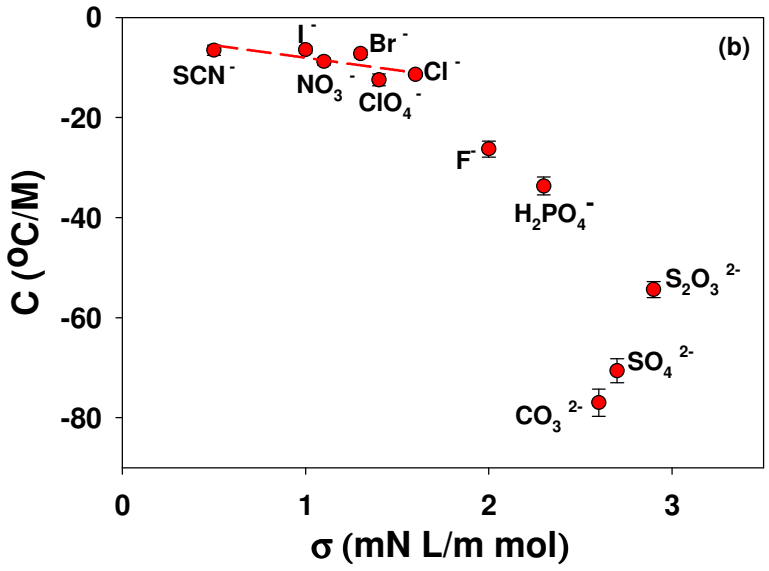

Figure 2.5. Plot of the linear slope, *c*, from eqn. 2.2 against (a) ΔS_{hydr} and (b) σ for ELP V_5-120 with 11 different sodium salts. The dashed red lines are fits to the kosmotropes in (a) and the chaotropes in (b).

In addition to the linear portion of the LCST vs. salt concentration curves shown in Figure 2.4, there is also a non-linear portion for the chaotropic anions. This can be directly visualized by subtracting out the linear contribution to the curves in Figure 2.4 and replotting the data (Figure 2.6). The binding isotherms are clearly revealed by this procedure. Significantly, they show a reasonably good fit to a Langmuir isotherm (dashed lines).

LCST of ELP $V_5A_2G_3$-120 with Hofmeister Salts

A slightly less hydrophobic biomacromolecule, ELP $V_5A_2G_3$-120, was chosen for a second set of experiments in order to ascertain the dependence of the LCST behavior on the amino acid sequence of the ELP. The polymer chain length of ELP $V_5A_2G_3$-120 was the same as ELP V_5-120, but half of the valine residues were replaced with glycines and alanines. Again, temperature dependent aggregation behavior was measured in the presence of the same 11 Hofmeister salts to directly compare the LCSTs values with ELP V_5-120 (Figure 2.7). As can be seen, the general trends are similar to those seen for ELP V_5-120. The data were again fit with eqns. 2.1 and 2.2 and the associated values of c, K_A, and B_{max} are provided in Table 2.1 on page 31. Furthermore, the correlation between the c values of the kosmotropes and ΔS_{hydr} was excellent (Figure 2.8a). The correlation between σ and the c values for the chaotropes was also quite good (Figure 2.8b). Finally, the residual portion of the LCST vs. salt concentration curves are plotted for the chaotropic ions in Figure 2.9 after the linear portions were subtracted out. Again, the data show evidence for a saturation binding phenomenon. The dashed lines in this figure are the apparent fits to the Langmuir isotherm equation.

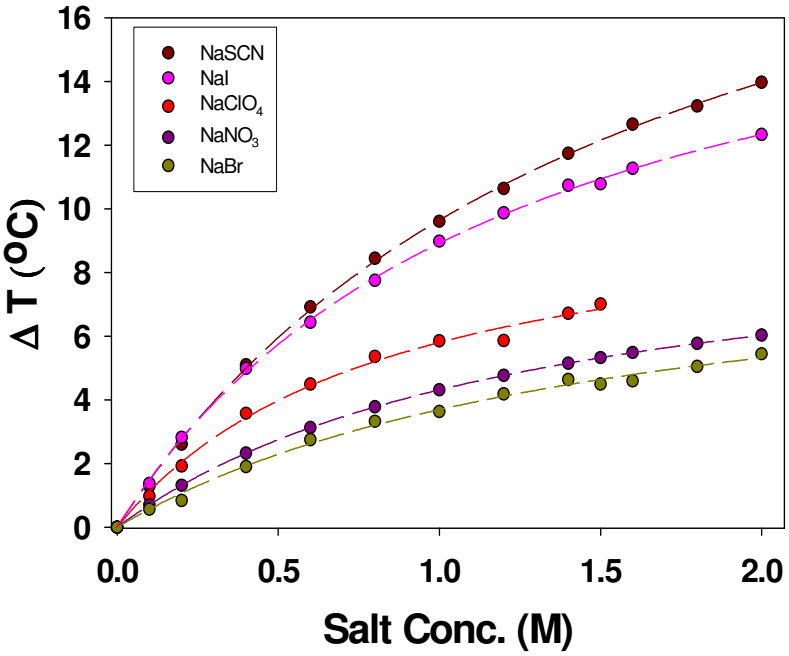

Figure 2.6. Residual LCST vs. salt concentration data for the chaotropic anions with ELP V_5-120 after subtracting out the linear portion of the data. The dashed lines represent Langmuir isotherm fits to the data points.

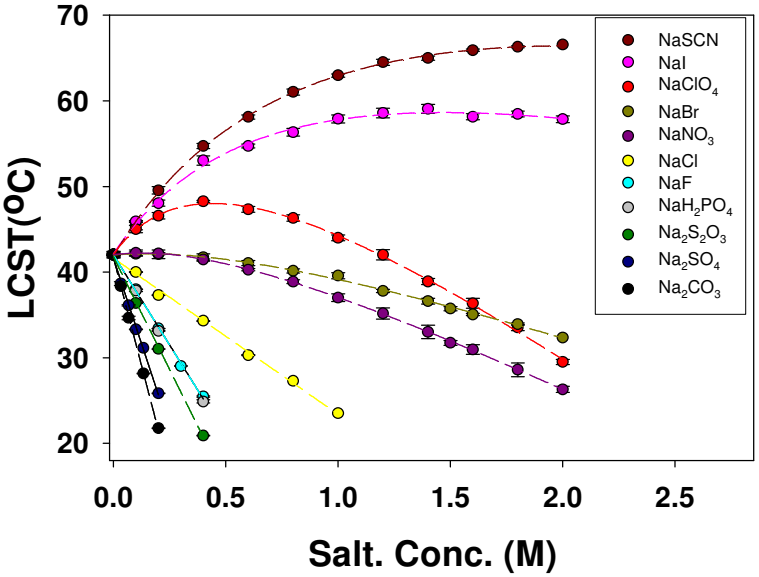

Figure 2.7. LCST vs. salt concentration curves for ELP $V_5A_2G_3$-120 with a series of sodium salts. Each data point represents the average of 8 measurements and the standard deviations are within the size of the circles used to plot the data. The dashed lines are fits to the data using eqns. 2.1&2.2.

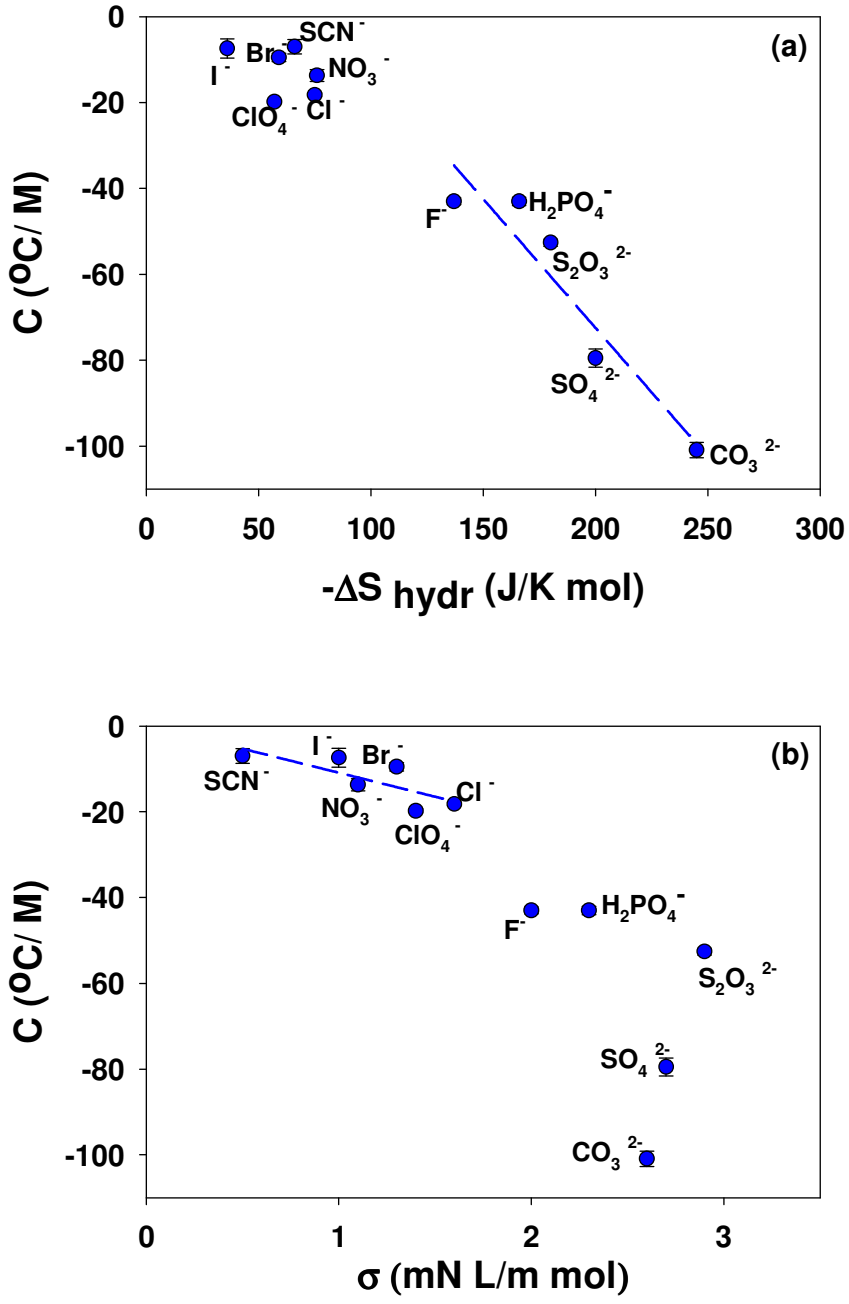

Figure 2.8. Plot of the linear slope, *c*, from eqns. 2.1& 2.2 against (a) ΔS_{hydr} and (b) σ for ELP $V_5A_2G_3$-120 with 11 different sodium salts. The dashed blue lines are fits to the kosmotropes in (a) and the chaotropes in (b).

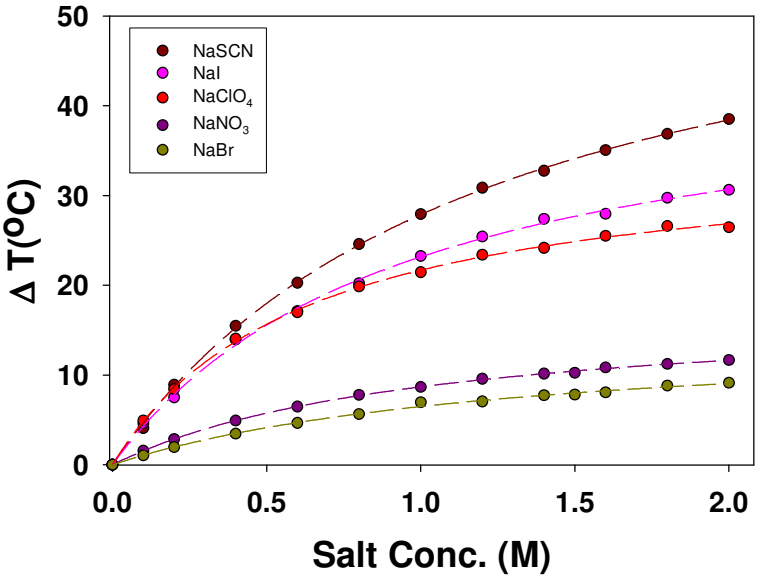

Figure 2.9. Residual LCST vs. salt concentration data for the chaotropic anions with ELP $V_5A_2G_3$-120 after subtracting out the linear portion of the data. The dashed lines represent Langmuir isotherm fits to the data points.

Discussion and Conclusion

Mechanisms for Modulating the LCST of ELPs by Salts

The data shown in Figures 2.4-2.9 are consistent with the mechanism for modulating the LCST of ELPs by Hofmeister anions presented in Figure 2.1. Specifically, kosmotropic ions modulate the phase transition temperature through the polarization of water molecules in the first hydration shell of the biopolymer (Figure 2.1a). Evidence for this statement comes from Figures 2.5a and 2.8a, which show that changes in the LCST are directly correlated to the entropies of hydration of the kosmotropes, but not for the chaotropes. Indeed, kosmotropic anions are well hydrated and are able to strongly attract protons of water molecules in their first hydration shell. This, in turn, leaves the rest of the water molecule more negatively charged. If the same water molecule is also hydrogen bonded to the amide group of the ELP, then the bond should be weakened by the polarization effect. This ability of kosmotropes to polarize water molecules is manifest at the macroscopic level by their ability to order water molecules around themselves and thereby lower the entropy of the aqueous solution, ΔS_{hydr}. By contrast, the chaotropes cannot sufficiently polarize polymer-associated water molecules to weaken the hydration of the amide moieties. Instead, the depression of the LCST comes from the destabilization of hydrophobic hydration waters. Evidence for this statement can be found in Figures 2.5b and 2.8b. As can be seen, there is a linear correlation between the surface tension increment of the chaotropic anions and the corresponding *c* value.

As noted above, the water polarization effect for kosmotropes and the surface tension increment effect for chaotropes are expected to cause the LCST of the ELPs to decrease linearly with salt concentration. This should be the case for the chaotropes because the surface tension of aqueous interfaces varies linearly with salt concentration.[15,27] Furthermore, one might also expect the polarization effect to be linearly dependent on the concentration of salt because no specific binding sites are involved.[11,15,28] On the other hand, the nonlinear component of the salting-in effect for the chaotropes follows saturation binding behavior (Figure 2.6 and 2.9). This is consistent with the notion that the amide dipoles serve as putative binding sites for these anions. Such binding interactions will increase the charge on the biomacromolecule and thereby inhibit hydrophobic collapse. It should be noted that the K_A values found for this system should be treated as only apparent association constants. Indeed, the measured LCST values for a given salt can vary by almost 30 ºC as the salt concentration is increased with ELP $V_5A_2G_3$-120 (Figure 2.7). Therefore, the experiments are not conducted isothermally. Moreover, binding should be anti-cooperative because it should become increasingly difficult to bind larger numbers of anions to the same polymer chain on electrostatic grounds.[29] Nevertheless, the residual curves abstracted in Figures 2.6and 2.9 are in reasonably good agreement with previous measurements of anion binding to amide moieties.[10] Specifically, the K_A values are in the same range as previous results. Also, the finding that more chaotropic anions bind more tightly than less chaotropic anions is in agreement with previous results.

Finally, Cl^- represents a somewhat anomalous case. Although the change in the LCST as a function of the NaCl concentration was linear like the kosmotropes (Figures 2.4 and 2.7), the thermodynamic correlation for Cl^- was to σ, like the chaotropes (Figures 2.5b and 2.8b). In other words, this ion's ΔS_{hydr} is sufficiently small that it does not cause induced polarization effects. However, the ion is sufficiently well hydrated that it does not noticeably bind to the polypeptide chains like the chaotropes. Thus, this ion represents intermediate behavior.

Comparison with PNIPAM

As noted above, our laboratory has previously measured the effects of Hofmeister salts on the LCST of PNIPAM.[16] The data for ELPs fit to the same sets of equations as PNIPAM with the same correlations amongst c values, ΔS_{hydr}, and σ. Moreover, a Langmuir isotherm fits the nonlinear portions of the chaotropic data. Such remarkable similarities speak to the general nature of our proposed mechanism for the modulation of hydrophobic collapse of uncharged polymers by salts.

In addition to similarities, there are also some significant differences between the behavior of ELPs and PNIPAM in the presence of salts. Most importantly, PNIPAM undergoes a two step collapse process in the presence of sufficient concentrations of kosmotropic ions.[16,24] For example, in the presence of 200 mM Na_2SO_4, a 10 mg/mL solution of PNIPAM undergoes partial collapse near 24 ºC and full collapse above 26 ºC. The partial collapse to a molten globule state manifests itself as a level of light scattering from the polymer solution which is intermediate between the high level found upon full hydrophobic collapse and the relatively low level that exists when the polymer solution

is below the LCST. In contrast with the PNIPAM data, no evidence was found in the present study for a thermodynamically stable molten globule state for the ELPs.

The partial collapse of PNIPAM was interpreted to arise from the separate dehydration of the amide moieties and the hydrophobic portions of the macromolecule. Evidently, the hydration waters could be removed from the amide moieties while the hydrophobic hydration waters remained intact. Corroborating evidence for this hypothesis came from subsequently performed NMR studies.[30] The key difference between the chemical structures of PNIPAM and the ELPs is the fact that the amide groups are pendent in acrylamide polymers, but part of the backbone in polypeptides. Apparently, when the amide groups are part of the backbone, removal of their hydration waters necessarily triggers the removal of hydrophobic hydration waters as well. On the other hand, when amide groups are pendent, the two processes can be decoupled.

ELP V_5-120 vs. ELP $V_5A_2G_3$-120

Both biopolymers investigated in the present study showed similar qualitative phase transition behavior as the specific ion identity and concentration were modulated. Nevertheless, there appears to be some key differences in the behavior of the two systems. For example, the LCST value, T_0, of ELP $V_5A_2G_3$-120 without added salt is about 14 ºC higher than that of ELP V_5-120. This is due to the presence of less hydrophobic residues such as alanine and glycine. Moreover, the *c* values were generally greater for $V_5A_2G_3$-120 than for the more hydrophobic V_5-120 biopolymer. This trend was found with both the kosmotropes and chaotropes. Such a universal trend almost

certainly reflects a more favorable partitioning of ions from bulk solution to the aqueous/polymer interface with the less hydrophobic polymer.[31]

More chemically specific information about the two polymers can be inferred by examining differences in B_{max} values for the chaotropic anions. Specifically, the higher values of B_{max} for ELP $V_5A_2G_3$-120 should be correlated with a larger number of bound anions.[24] This is consistent with the more open structure of the polymer. However, the magnitude of the difference between the two polymers should be ion specific and depend upon the ionic volume for a given chaotropic anion. For sufficiently small anions, the effect should be rather limited as they would be able to equally access binding sites on both polymers. On the other hand, bigger ions should be more strongly inhibited from binding to at least some sites on ELP V_5-120 in comparison with the more open ELP $V_5A_2G_3$-120 construct.

To help quantify ion specific differences in binding site accessibility, the ratios of B_{max} values for the two polymers are provided in Table 2.1 [$B_{max}(V_5A_2G_3)/B_{max}(V_5)$]. A plot of this ratio against the ionic volume of each of the chaotropic anions is provided in Figure 2.10. As can be seen, a linear trend between the B_{max} ratio and ionic volume is observed. As expected, the largest anion, ClO_4^-, has the largest ratio, while the effect of Br^- is more modest. Moreover, it appears that there is a cutoff for this effect around an ionic volume of 25 cm^3/mol. In other words, binding for anions with volumes below this particular size would be expected to have a B_{max} ratio of 1.0.

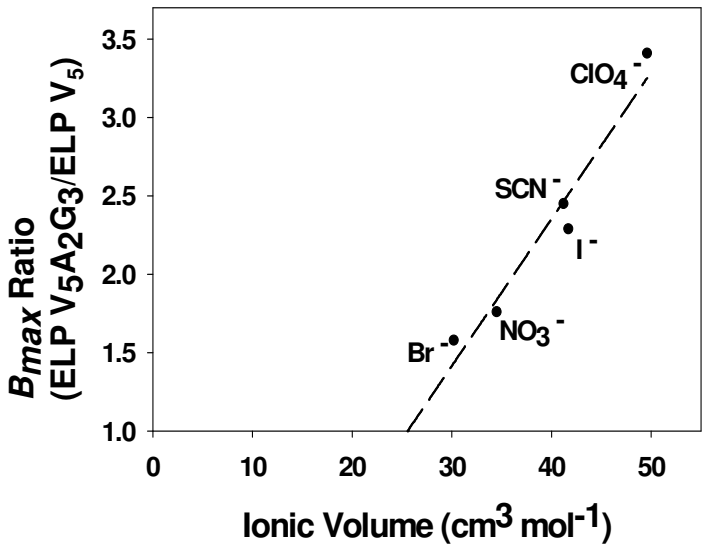

Figure 2.10. Plot of the ratio of B_{max} values for ELP $V_5A_2G_3$-120/ ELP V_5-120 vs. ionic volume of chaotropes ions.

Table 2.1: Fitted values from LCST data of ELP V_5-120 and ELP $V_5A_2G_3$-120 with 11 sodium salts to eqns 2.1 and 2.2. B_{max} has about 10% error while the errors on the K_A values are smaller.

Ion	ELP V_5-120			ELP $V_5A_2G_3$-120			ELP$V_5A_2G_3$-120/ ELP V_5-120
	B_{max}	K_A	c	B_{max}	K_A	c	B_{max} ratio
SCN^-	25.1	0.63	-6.6± 1.0	61.5	0.84	-7.0±1.7	2.5
I^-	19.9	0.81	-6.5±0.7	45.7	1.0	-7.4±2.2	2.3
$ClO4^-$	10.6	1.3	-12.5±0.8	36.4	1.5	-20±1.0	3.4
Br^-	9.38	0.67	-7.3±0.7	14.8	0.78	-9.4±1.4	1.6
NO_3^-	10.0	0.76	-8.8±1.2	17.6	0.97	-14±0.5	1.8
Cl^-	-	-	-11.4±0.4	-	-	-18±0.5	-
F -	-	-	-26.3±1.6	-	-	-43±0.8	-
$H_2PO_4^-$	-	-	-33.7±1.8	-	-	-43±1.0	-
$S_2O_3^{2-}$	-	-	-54.4±1.6	-	-	-53±0.8	-
SO_4^{2-}	-	-	-70.6±2.4	-	-	-79±2.1	-
CO_3^{2-}	-	-	-77.0±2.7	-	-	-100±1.8	-

CHAPTER III

SPECIFIC ANION EFFECTS ON PHASE TRANSTION TEMPERATURES OF POSITIVELY CHARGED ELASTIN-LIKE POLYPEPTIDES

Introduction

In our previous report, Hofmeister anion effects on the LCST of two neutral elastin-like polypeptides (ELPs) were studied (Chapter II).[32] First, the salting-out mechanism of kosmotropes were found to be due to the polarization effects of strongly hydrated kosmotropic anions on the water molecules that are specifically hydrogen bonded to the polymers. Salting-out effects of chaotropic anions are due to surface tension increment around the exposed hydrophobic surfaces on the polymers. Lastly, the salting-in effects of chaotropic anions are due to the direct interaction of anions with the polypeptides.

When the macromolecules are positively charged, an inverse Hofmeister series is observed.[33] In other words chaotropic anions show a greater salting-out effects than kosmotropic anions. To investigate this we employed ELP KV_6-112 as a model system. ELP KV_6-112 has 16 lysine residues in the guest residue position and the pI of the polypeptide is 10.0 which make the polypeptides positively charged at pH 7.0. Interestingly, we observed both inverse and direct Hofmeister effects on the phase transition of ELP KV_6-112. When the salt concentration was low, the orders of Hofmeister anions were inversed and as the concentration of salt increases, the direct Hofmeister anions series has shown. The result of this study was also compared to the result of previous study with two neutral systems.

Experimental

ELP preparation and LCST measurements are same as described in Chapter II for neutral ELPs.

Results

Overall plot of LCST vs. salt concentration with ELP KV_6-112 is shown in Figure 3.1. The LCST of 6.4 mg/mL of ELP KV_6-112 was measured with different concentrations of six monovalent salts.

The initial LCST without salt is 72 ^{o}C. The initial LCST drops exponentially in the low salt concentration regime which is due to the screening of positive charge on the polypeptide by anions. In the low salt concentration region of the LCST plot, an inverse Hofmeister series of anions was observed i.e., the most chaotropic anions showed the greatest salting-out effects. However, the order of the anions gets reversed at the high salt concentration region. With a high salt concentration, the direct Hofmeister series is shown where the most kosmotropic anion Cl^- showed the most salting-out effect. Interestingly, the LCST of the polypeptide increased at high concentrations of SCN^- and I^-.

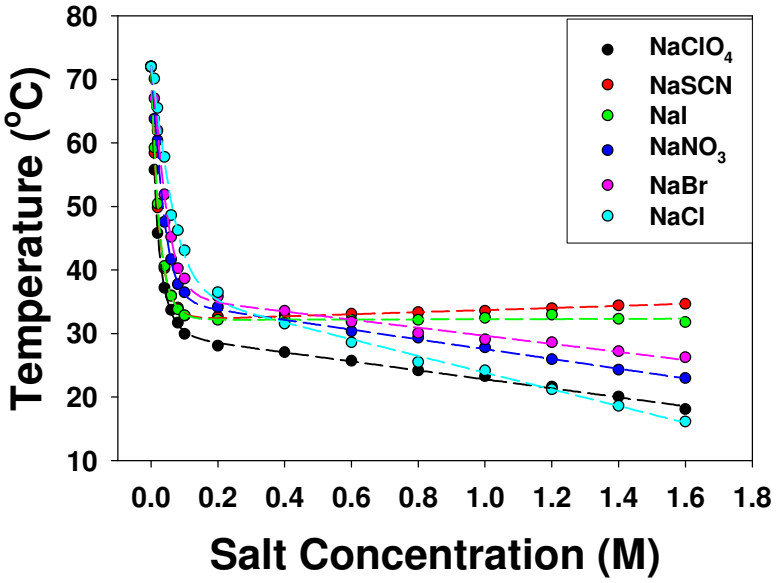

Figure 3.1. LCST vs. salt concentration curves for a series of sodium salts with ELP KV_6-112. Each data point represents the average of 8 measurements and the standard deviations are within the size of the circular data points in all cases. The dashed lines are fits to the data using eqn. 3.1.

Modeling the LCST vs. Salt Concentration Data

The overall LCST vs. salt concentration plot in Fig 3.1 can be fitted with equation 3.1. The first part of equation 3.1 is a modified version of Langmuir isotherm which describes the specific association of anions to the polypeptides. An exponential term is added to the Langmuir isotherm binding equation to take account for an electrostatic interaction between the negatively charged anions and the positively charged ELP. The second term in the equation is a simple linear equation describing the ions ability to alter the surface tension of water around the polypeptides.

$$T = T_0 + \frac{B_{\max}[M]e^{-b[M]}}{K_d + [M]e^{-b[M]}} + c[M] \qquad (3.1)$$

It has been shown that surface tension at the air-water interphase is changed linearly upon the addition of ions.[34] The dashed lines in Fig. 3.1 are fits to the data with eqn. 3.1. T_0 is the LCST of the ELP without salt, and [M] is the concentration of salt in molarity. The constant B_{max} has units of temperature and represents the maximum increase in LCST when anions are associated with all of the positively charged residues. The constant, b, has units of reciprocal molarity and is an electrostatic interaction factor that is related to the surface potential of ELP. B_{max} and b represents anions ability to associate with positive charges on the ELP surface result in decrease in electrostatic repulsion between the positive lysine residues. The constant, c, has units of temperature/molarity and represents specific anion effects on the interfacial tension at the ELP/water interface.

It should be noted that the fitting equation 3.1 is a modified version of the equation 2.2 which used to fit the neutral model system. In case of neutral system, b = 0 and the exponential term becomes 1 which simplifies the equation. The fitting parameters, *Bmax, b, c*, and Kd are presented in Table 3.1 on page 47.

For a further analysis, fit to the binding and the linear part of the data was plotted separately. First, binding data was plotted for a quantitative analysis on electrostatic interactions between the negatively charged anions and positively charged polypeptides (Figure 3.2). The initial LCST vs. salt concentration data followed an inverse Hofmiester series. The chaotropic anions which usually involved in salting-in effects showed a greater salting-out behavior in case of LCST of ELP KV_6-112. The initial drastic salting-out behavior was saturated at a 200 mM salt concentration. The residual linear data after subtracting the binding data was plotted (Fig. 3.3). Interestingly, anions in this plot followed a direct Hofmeister series. Relatively kosmotropic anion, Cl- , showed the greatest salting-out behavior among the anions and the LCST of ELP KV_6-112 was increased at high concentrations of SCN^- and I^- .

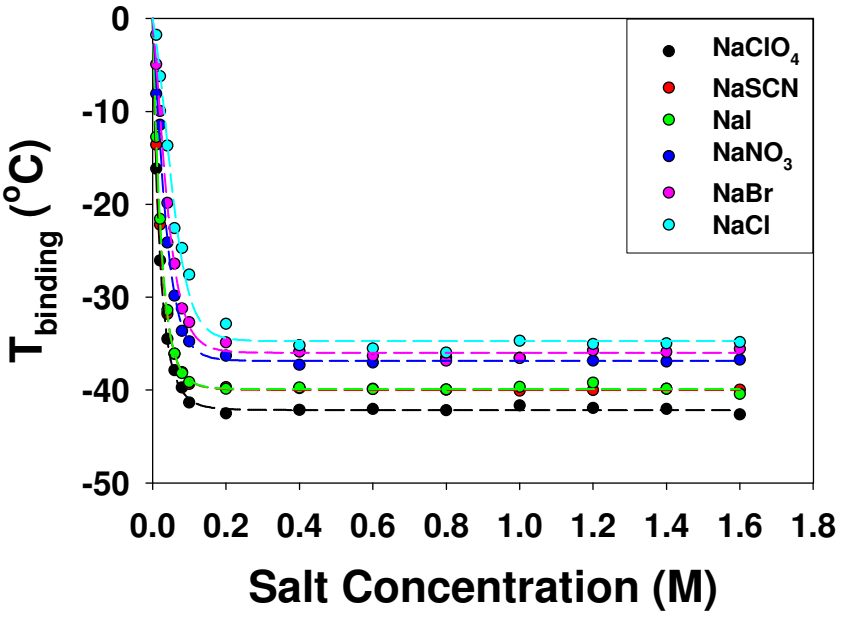

Figure 3.2. The inverse Hofmeister series of anions with ELP KV_6-112. The residual LCST data from Fig. 3.1 after subtracting the linear portion of the curves. The lines represent fits to the data points by binding term.

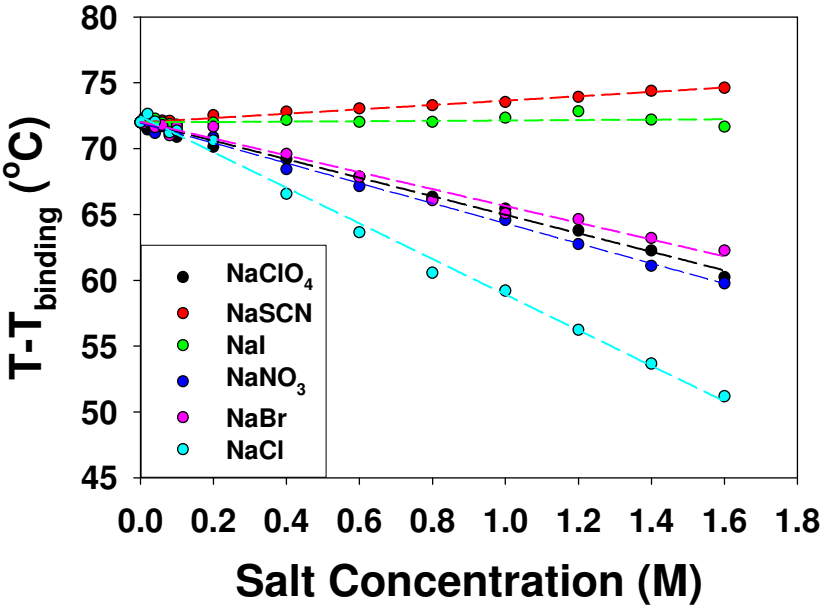

Figure 3.3. The direct Hofmeister series of anions with ELP KV_6-112. The residual LCST data after removing the binding term. The lines represent linear fits to the data points.

Discussion and Conclusion

Direct Interaction Between Anions and the Polypeptides

As it can be seen in Figure 3.2, the initial exponential drop of LCST follows an inverse Hofmeister series. The explanation for this is based on the change in surface potential of the ELP. The initial LCST of the polypeptide is relatively high compared to the neutral ELPs of similar chain lengths due to the charge repulsion from the positively charged lysine groups at pH 7.0. Upon the addition of the negatively charged anions in the solution, the direct interaction of the anions with the positively charged polypeptides neutralizes the overall positive charge on the ELP which in turn lowers the surface potential of the ELP. This lowering of the surface potential of ELP makes it easier to collapse.

The B_{max} values abstracted from fits to the data can be correlated with partial molar volumes (V_i^0) of the anions.(Figure 3.4(a)) The partial molar volume of anions describes the size of hydrated anions in aqueous solution. As it can be seen in Figure 3.4, larger anions have greater effects on B_{max} values. In other words, larger anions are more effective in salting the polypeptides out of solution by screening the positive charges on the ELPs. The B_{max} values from the fit also show a nice correlation with ΔG_{hydr} of anions (Figure 3.4(b)). This is reasonable since the partial molar volume V_i^0 for a given anion in aqueous solution is directly proportional to its hydration free energy. The free energy of hydration of anions is the differences in energy of anions from a fixed point in vacuum to a fixed point in the solution.

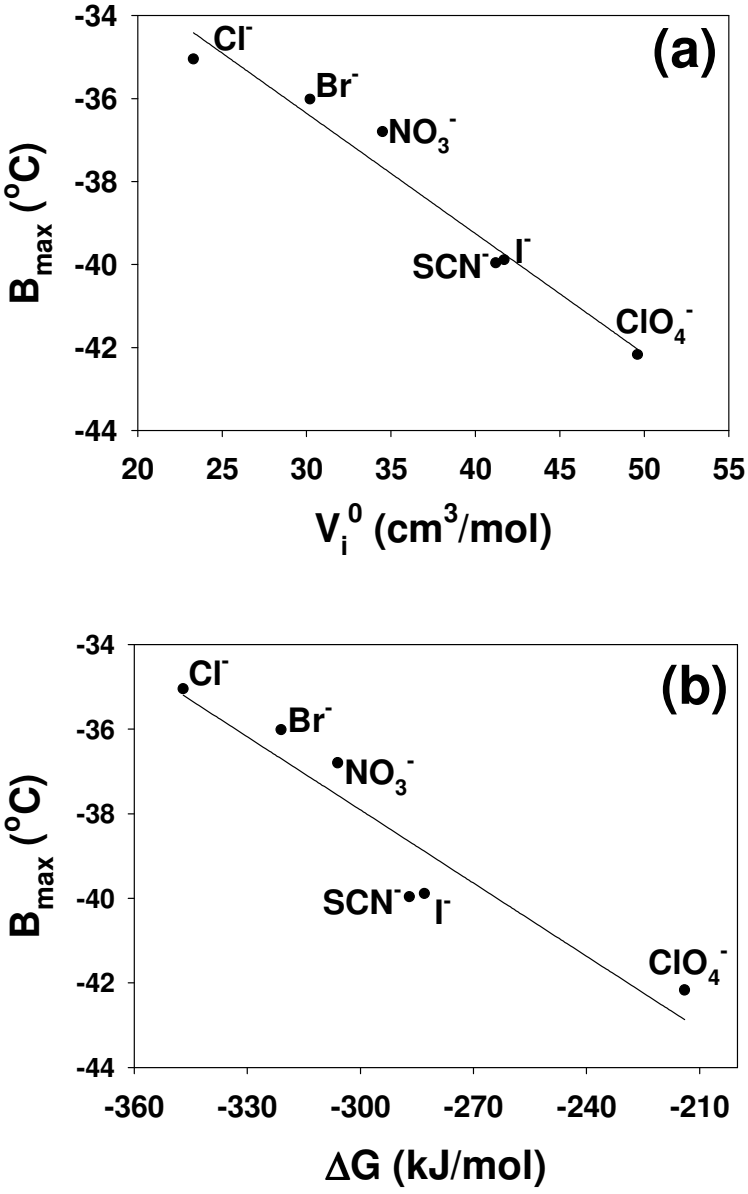

Figure 3.4. (a) Plot of partial molar volume of anions vs. constant B_{max} for ELP KV_6-112. (b) Plot of Gibbs free energy of hydration of anions vs. constant B_{max} for ELP KV_6-112.

The inverse Hofmeister series of ELP KV_6-112 can be explained based on the anions ability to associate with positively charged lysine residues on the polypeptides. Bigger anions which can shed their hydration layer easier can directly interact with the lysine residue to neutralize the positive surface charge on the ELP. Usually chaotropic anions in the Hofmeister series are larger in volume than kosmotropic anions therefore, chaotropic anions shows a greater salting-out effects of ELP KV_6-112 trough screening of charge on the polypeptide.

Unlike the correlation plot with B_{max} values, there was no linear correlation with *b* values of anions and the partial molar volume of anions (Figure 3.5(a)) or the free energy of hydration of anions (Figure 3.5(b)). Especially the *b* value of ClO_4^- is higher than most of the anions except Cl^-. Since perchlorate is a round shaped, bulky anion, it might interact with more than one lysine residue at a time. The salting-out effects of this anions is greater than other chaotropic anions such as SCN- or I-. There was no salting-in effects from ClO_4^- at least up to the 1.6 M salt concentration.

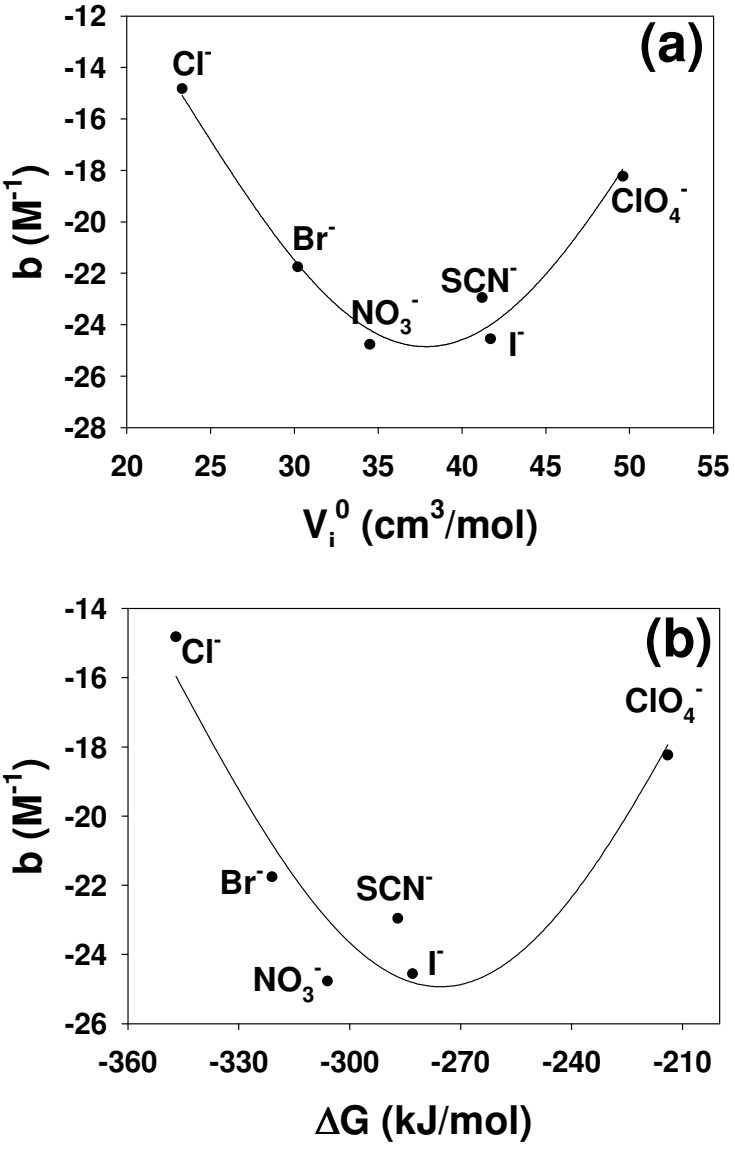

Figure 3.5. (a) Plot of partial molar volume of anions vs. constant *b* for ELP KV_6-112. (b) Plot of Gibbs free energy of hydration of anions vs. constant *b* for ELP KV_6-112.

Anion Effects on Surface Tension

The second part of the Hofmeister effects on LCST of ELP KV_6-112 is based on the anions ability to alter the surface tension around the polypeptides. As can be seen in Figure 3.3, the residual data after subtracting the binding part from the overall LCST vs. salt concentration data shows a linear behavior. It is well known that the surface tension at the air/water interface varies linearly with salt concentration up to at least moderate ionic strengths. With the exception of SCN^- and I^-, all the other anions shows a further salting-out behavior which is represented by a negative slope in Figure 3.3. Interestingly, the mechanism for this linear behavior of LCST upon the salt concentration shares the same mechanism as for the salting-out of chaotropic anions with neutral ELPs. In our previous study with two neutral ELPs that are similar in chain length as ELP KV_6-112, a salting-out mechanism of chaotropes was explained based on their ability to alter the surface tension of hydration layer around the exposed hydrophobic moiety of the polypeptides. We also observed a nice linear correlation between the c values from the fitting and surface tension increment of anions for ELP KV_6-112 (Figure 3.6). The anions that increases the surface tension, Cl^- ClO_4^-, Br^-, and NO_3^- lowers the LCST further after the initial binding to the positively charged residues on the polypeptides has occurred.

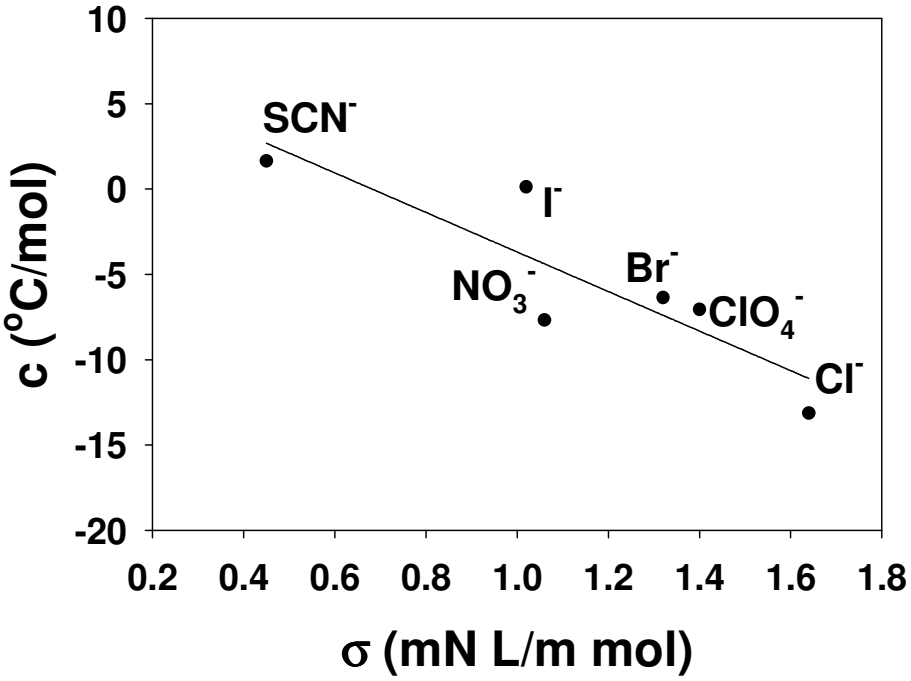

Figure 3.6. Plot of surface tension increment values of anions vs constant *c* for ELP KV_6-112.

ELP KV_6-112 vs. Neutral ELPs

The mechanism for the specific anion effects on the phase transition temperature of ELP KV_6-112 is based on the ionic volume and the surface tension increments. In the low salt concentration region, an exponential decrease in LCST is observed with all salts. Charge neutralization effects of anions that are directly interacting with positive charge moieties on the polypeptide lowers the surface potential of the ELP which makes it easier to collapse. This behavior is more pronounced with bigger anions so an inverse order of Hofmeister series was observed. As the concentration of salt increases, SCN-, I- shows a saturation behavior where the change in LCST becomes small or the LCST starts to increase in case of SCN-. On the other hand, other anions such as Br^-, NO_3^-, Cl^- ClO_4^- shows a further decrease in LCST even after several hundred mM of salt concentration. This part of the data showed a strong correlation with ions ability to alter the surface tension of hydration layer around the polypeptide. Once the overall charge on the polypeptides is neutralized with association of anions, the specific anions effects on the LCST of ELP KV_6-112 shows a very similar behavior as the neutral ELPs. In our previous study, chaotropic anions on the phase transition temperature of ELPs showed an initial salting-in behavior due to a direct interaction of anions with the polypeptides followed by salting-out effects due to the surface tension increment of the anions. Here, we used a charged ELP to incorporate the charge-charge interaction and was able to observed the general behavior of anions once the overall charge is neutralized.

Probing Other Systems

The data from ELP V_5-120, $V_5A_2G_3$-120, and ELP KV_6-112 clearly show that ELPs can be employed to glean information about specific ion effects on hydrophobic collapse. The fact that the fourth residue in the pentameric repeat is a guest residue holds out the very promising prospect for investigating the influence of specific residues on Hofmeister behavior. For example, the addition of other charged residues such as D, E, and R should allow screening effects for both cationic and anionic polymers to be considered. On the other hand, the use of F residues would be advantageous for the investigation of cation-π interactions. Exactly these types of investigation are presently underway in our laboratories.

Table 3.1: Fitted values from LCST data of ELP KV_6-112 with 6 sodium salts to eqn. 3.1.

Ion	B_{max} (^oC)	$B(M^{-1})$	$C(^oC/mol)$	K_d (M)
ClO_4^-	-42.2	-18.2	-7.05	0.0185
SCN^-	-39.9	-22.9	1.64	0.0250
I^-	-39.8	-24.5	0.13	0.0276
NO_3^-	-36.7	-24.7	-7.67	0.0599
Br^-	-36.0	-21.7	-6.35	0.0785
Cl^-	-35.0	-14.8	-13.1	0.105

CHAPTER IV

SOLVENT ISOTOPE EFFECTS ON PHASE TRANSITION TEMPERATURES OF ELASTIN-LIKE POLYPEPTIDES

Introduction

Understanding protein stability and folding is of central importance in chemistry, biology, and medicine. Solvent isotope effects have provided important clues about the stability of various structural units found in folded proteins. Specifically, previous studies comparing protein stability in D_2O vs. H_2O have shown that the folded state is often, but not always stabilized in D_2O.[35] For example, proteins possessing mostly β-type structures are preferentially stabilized in D_2O, while α– helical structures show the opposite trend.[36] These observations are usually attributed to one of two effects: (1) D_2O strengthens hydrophobic interactions in proteins inducing hydrophobic collapse; or (2) D_2O selectively stabilizes inter and/or intra molecular hydrogen bonds which are more prevalent in the folded state of protein.[37]

In order to access the relative contributions of hydrogen bonding and hydrophobic interactions on β-structure, one must be able to tailor both effects separately (Figure 4.1).

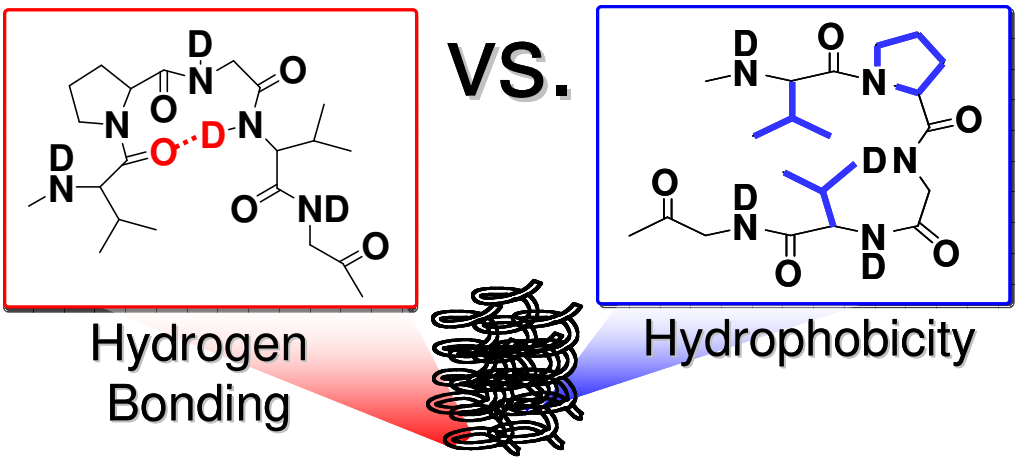

Figure 4.1. Schematics of intra molecular hydrogen bond in b-turn structure of VPGVG pentapeptide repeat of ELPs and hydrophobic side chains in the ELP.

Unfortunately, due to the inherent complexity of proteins, systematically altering global hydrophobicity through mutagenesis without changing protein structure is an extraordinarily difficult task.[38] Herein; we show that the hydrogen bonds in at least one class of polypeptides are stabilized relative to hydrophobic interactions upon switching from H_2O to D_2O. These biomacromolecules belong to a family of elastin-like polypeptides (ELPs) that consist of the pentapeptide repeat unit Val-Pro-Gly-Xaa-Gly, where Xaa can be any residue except proline. Upon raising the temperature, ELPs undergo hydrophobic collapse accompanied by an increase in secondary/tertiary structure formation much like folded proteins.[39] The temperature at which this transition occurs is referred to as the lower critical solution temperature (LCST).[40] Although the structure of the collapsed state of ELPs has not been completely determined, it is believed to involve β-spiral formation, which consists of type II β-turns arranged in a helical fashion with intraspiral hydrophobic contacts.[39,41]

Unlike structured proteins, the hydrophobicity of ELPs can be systematically tuned by simply replacing the guest residues with more or less hydrophobic amino acids or by changing the chain length of an otherwise identical sequence.[18,42] Thus, we have compared the LCST of ELPs of different amino acid compositions and chain lengths in H_2O and D_2O. The five ELP's employed in this study were: ELP V_5-120, QV_6-112, $V_5A_2G_3$-330, $V_5A_2G_3$-120, and $V_5A_2G_3$-60. ELP V_5-120 contains valine (V) residues in the guest sites and therefore consists of 120 repeats of VPGVG for a total of 600 residues. By contrast, ELP $V_5A_2G_3$-60 contains 300 total residues whereby valine,

alanine (A), and glycine (G) are present in the X position in a ratio of 5:2:3. ELP QV_6-112 contains 560 residues in which glutamine (Q) and V are present in a 1:6 ratio.

Experimental

ELP Preparation

The pET plasmids of five ELPs were constructed by the recursive directional ligation method as previously described.[18] Expression of plasmids and purification of ELPs was also done following previously described procedures.[40] The plasmids were expressed in BLR/DE3 *E. coli* in TB dry media with the addition of ampicillin. The cells were expressed for 24 hr at 37 ^{o}C and then lysed by sonication. Purification of the ELPs accomplished via inverse phase transition cycling. After several cycles, samples were dialyzed against purified water (NANOpure Ultrapure Water System, Barnstead, Dubuque, IA) with a 18 MΩ·cm minimum resistivity to remove residual salts. The samples were lyophilized and stored at -80 ^{o}C until use.

LCST Measurements

Distilled and purified water (NANOpure Ultrapure Water System, Barnstead, Dubuque, IA) with a minimum resistivity of 18 MΩ·cm was used for all H_2O experiments. D_2O was purchased from Cambridge Isotope (>99.9% purity) and used without further purification. All ELP solutions were prepared in pure H_2O and D_2O without any additional salt at a polypeptide concentration of 6.4 mg/ml. The LCST values of the ELP solutions were measured with a microfluidic temperature-gradient apparatus placed under a dark field microscope as previously described.[40,43]

Circular Dichroism (CD)

Circular dichroism (CD) measurements were taken with an AVIV 62DS spectropolarimeter using a NesLab Coolflow CFT-33 refrigerated circulator. The conversion of CD signal, which is the difference in absorption minus the background, Δm, to mean residue ellipticity, $[\theta]_{obd}$ was done using the following equation:

$$[\theta]_{obd} = \frac{100 \cdot \Delta m}{C \cdot n \cdot l} \tag{4.1}$$

where C is the polypeptide concentration in mM, n is the number of residues in the polypeptide, and l is the path length in cm.[44] It should be noted that $[\theta]_{obd}$ has units of deg•cm^2/dmol. CD spectra were taken every 1 nm between 185 and 240 nm with 20 sec averaging times. Samples were degassed prior to each measurement and placed in a cuvette with a 1 mm path length. The random coil and β-turn structures were determined by monitoring the ellipticity near 198 nm and 210 nm, respectively, at 25 ºC in D_2O, and H_2O solutions.

Figure 4.3 in page 58 shows CD data for five ELPs in D_2O (green points) and H_2O (red points). As can be seen, the peak at 210 nm is greater in D_2O than H_2O for all five ELPs and the difference is more pronounced in more hydrophilic ELP such as ELP $V_5A_2G_3$-60. This difference goes to zero for the most hydrophobic polymer, ELP V_5-120.

Amide I Band ATR/FTIR Measurements

Fourier transform infrared (FTIR) spectra were taken with a Nicolet 470 FTIR spectrometer equipped with a liquid nitrogen cooled MCT detector (Thermo Electron

Corporation, Madison, WI) and a Pike Miracle attenuated total reflection (ATR) setup with a ZnSe (single bounce) crystal (Pike Technologies, Madison WI). Temperature of the sample stage was controlled with a circulation bath for measurements above the phase transition temperature of ELP samples. Sample volume of 120 μl was pipetted into Teflon well placed on top of ZnSe crystal and the cloudiness of sample solution was observed to insure the phase transition. 256 scans were accumulated per spectrum from 4000 to 400 cm^{-1}, at 2 cm^{-1} resolution. Background spectra were taken directly before the samples were probed and subtracted automatically from the sample data. For each sample containing ELP, spectra of pure D_2O solution was taken then subtracted from the first spectrum. Baseline correction was carried out in Matlab (Mathworks, Natick, MA) by subtracting polynomials in order to make the baseline flat around the peaks of interest. Spectral fitting was carried out in Matlab with frequencies restricted within a 10 cm^{-1} window, but with unrestricted linewidths. The quality of the spectral fits were judged by the least error sum method and all spectral fits shown have the lowest least error sum.

DSC Measurements

Differential scanning calorimetry data was taken with VP-DSC MicroCalorimeter (Microcal, LLC) with at a temperature ramping rate of 0.5^{o}C/min. All the solution was filtered with 0.2 μm syringe filter followed by degassing for 10 min prior to use. Pure H_2O and D_2O were used as a reference solution. Degassed sample and reference solution was loaded to the sample holder with a syringe to 500 μl. samples were cooled down to 15^{o}C and hold for 30min before the scanning began. Each

measurement was taken up to 15^{o}C above the transition temperature of sample solution. Baseline correction was done with an Origin program. Spectral fitting was carried out in Microsoft Excel with combination of Gaussian and Exponential. The quality of fit was judged by the least error sum method.

Results and Discussion

LCST of ELPs in D_2O and H_2O

The LCSTs of all the ELPs were found to be lowered in D_2O relative to H_2O (Table 4.1), indicating that the hydrophobically collapsed state was stabilized in D_2O. Intriguingly, the drop in the phase transition temperature in D_2O showed an inverse correlation with the hydrophobicity of the polypeptide. Thus, the ELPs which were most stabilized in D_2O possessed fewer hydrophobic amino acids or shorter chain length in the case of the three polypeptides of constant chemical composition. These LCST measurements strongly suggested that hydrophobicity was not the driving force for the relative stabilization of the collapsed state of the ELPs in D_2O.

It should be noted that the LCST of poly (*N*-isopropylacrymide) (PNIPAM), another thermoresponsive polymer, is higher in D_2O than that in H_2O.[45] As PNIPAM undergoes entropically driven hydrophobic collapse in a similar manner to ELPs, it is at least feasible that this difference arises solely due to the lack of structure in PNIPAM relative to ELP. While ELPs and most structured proteins contain approximately 60% intra and/or inter molecular hydrogen bonds in the collapsed state,[46] PNIPAM only contains ~10% hydrogen bonds.[47]

Table 4.1: LCST values of ELPs in H_2O and D_2O at 6.4 mg/mL.

	V_5-120	QV_6-112	$V_5A_2G_3$-330	$V_5A_2G_3$-120	$V_5A_2G_3$-60
LCST (H_2O)	28.5 ± 0.2	33.1 ± 0.2	40.6 ± 0.3	46.1 ± 0.2	50.7 ± 0.2
LCST (D_2O)	26.5 ± 0.2	30.4 ± 0.3	36.6 ± 0.2	40.9 ± 0.2	45.1 ± 0.2
Δ LCST	2 ± 0.3	2.7 ± 0.4	4.0 ± 0.4	5.1 ± 0.3	5.6 ± 0.3

Secondary Structure of ELPs by Circular Dichroism

Based on the above observations, we wished to investigate whether less hydrophobic and shorter ELPs (i.e. $V_5A_2G_3$-60) possessed greater amounts of secondary structure relative to more hydrophobic macromolecules (*i.e.*, V_5-120). Circular dichroism was employed to investigate such structural differences. All five ELPs were compared 5 ºC below their respective LCST values (Figure 4.2). As can be seen, less hydrophobic ELPs had significantly less random coil structure (smaller dip at 198 nm) and increased β-turn structure (higher peak at 210 nm) compared to the most hydrophobic ELPs. Consequently, we wondered if any structural enhancement could be observable with the same ELP in D_2O compared to H_2O. As shown in Figure 4.3, ELP $V_5A_2G_3$-60 had increased β-turn structure in D_2O.[21] Thus, the β-turn structure of this ELP appears to be stabilized in D_2O relative to H_2O. These trends are followed for all ELPs (Figure 4.3).

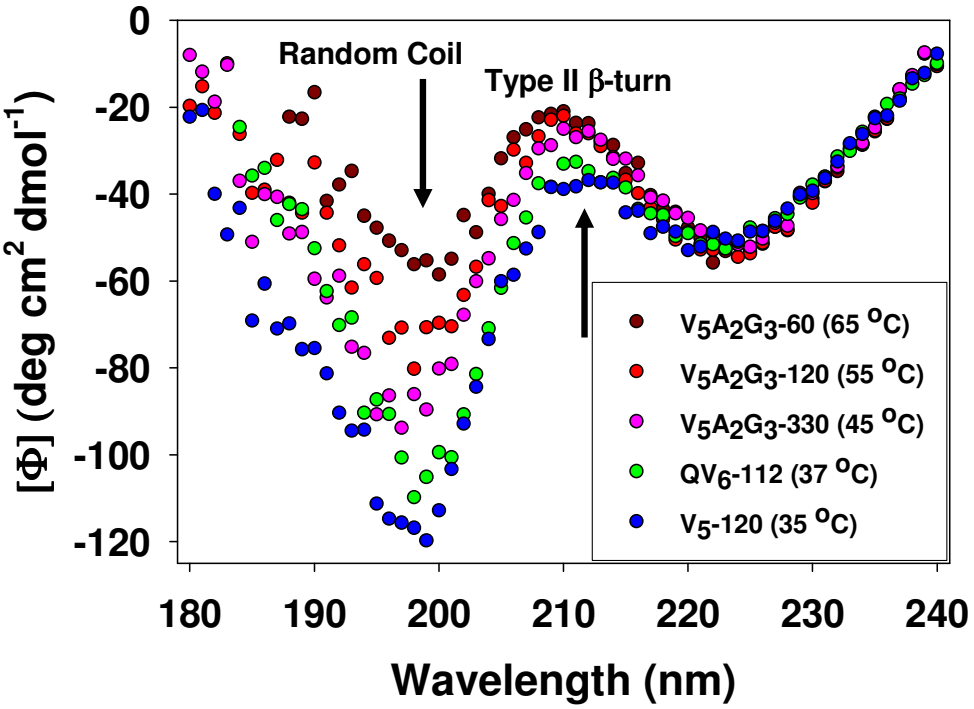

Figure 4.2. CD data for five ELPs with 0.16 mg/mL polypeptide concentration in H_2O. Spectrum is taken at 5 °C below their LCSTs.

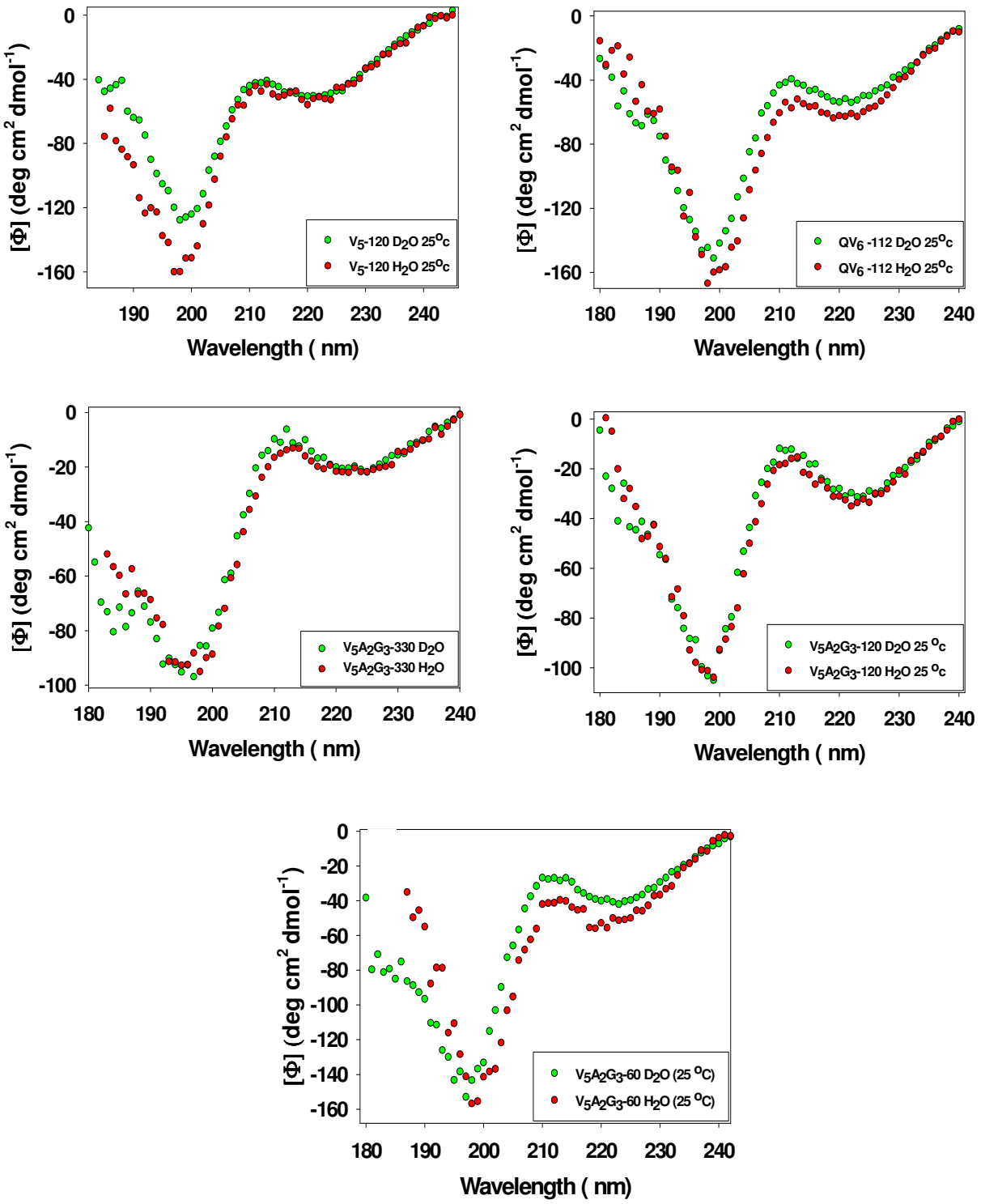

Figure 4.3. CD data for four ELPs with 0.16 mg/mL polypeptide concentration in H_2O and D_2O at 25°C.

Secondary Structure of Collapsed State ELPs by FTIR

In order to investigate structural changes in ELPs of increasing hydrophobicity in the collapsed state, Amide I Band ATR/FTIR studies were performed. Unlike CD, FTIR spectroscopy is particularly useful for probing structure in the collapsed state of the biopolymer since light scattering is not problematic at IR wavelengths. FTIR spectra were collected from all five ELPs above their LCSTs at the same concentration used to measure the LCST values shown in Table 4.1. The spectrum from V_5-120 is shown in Figure 4.4 as an example. There are two peaks at 1619 cm^{-1} and ~1663 cm^{-1} assigned to β-spiral structure (blue fits), while a third peak at ~1642 cm^{-1} is due to either β-sheet or, more likely, random coil structure (green fit).[48] Our results indicate that the less hydrophobic ELPs possessed greater amounts of β-spiral structure (Figure 4.4). Strikingly, there was a direct correlation between the difference in the LCST value of a given ELP in H_2O vs. D_2O and the amount of β-spiral structure observed by FTIR spectroscopy (Figure 4.5). Therefore, the formation of β-spiral structure can be directly linked to the relative stabilization of the collapsed state of the ELP in D_2O.

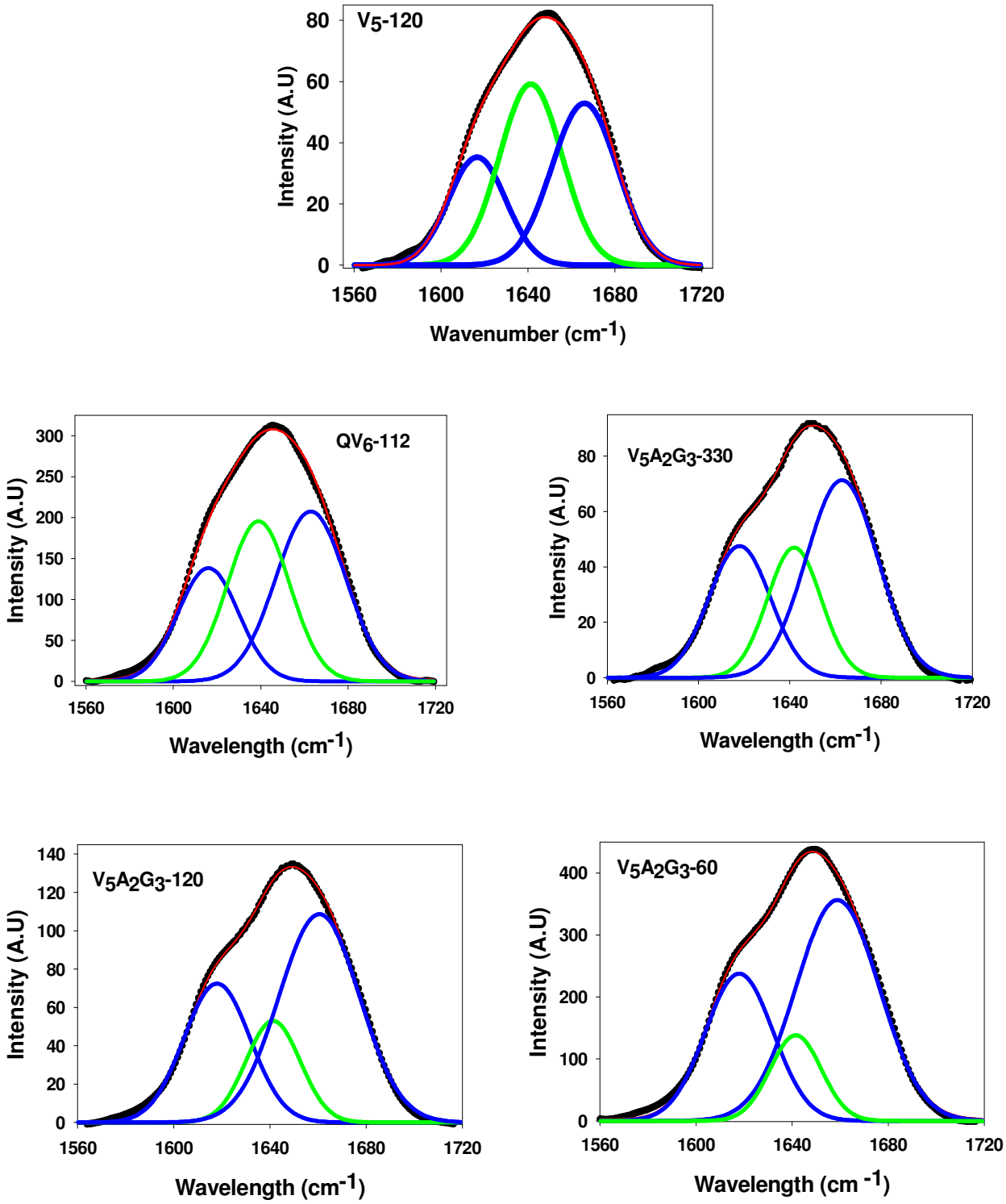

Figure 4.4. FTIR specturm of fourELPs in D_2O. Spectrum was taken at temperatures above their LCSTs. Black dotted line is original data, red line is the overall fitting, blue lines are fits for β-spiral structure, and green line is the fit for β-sheet/random coil.

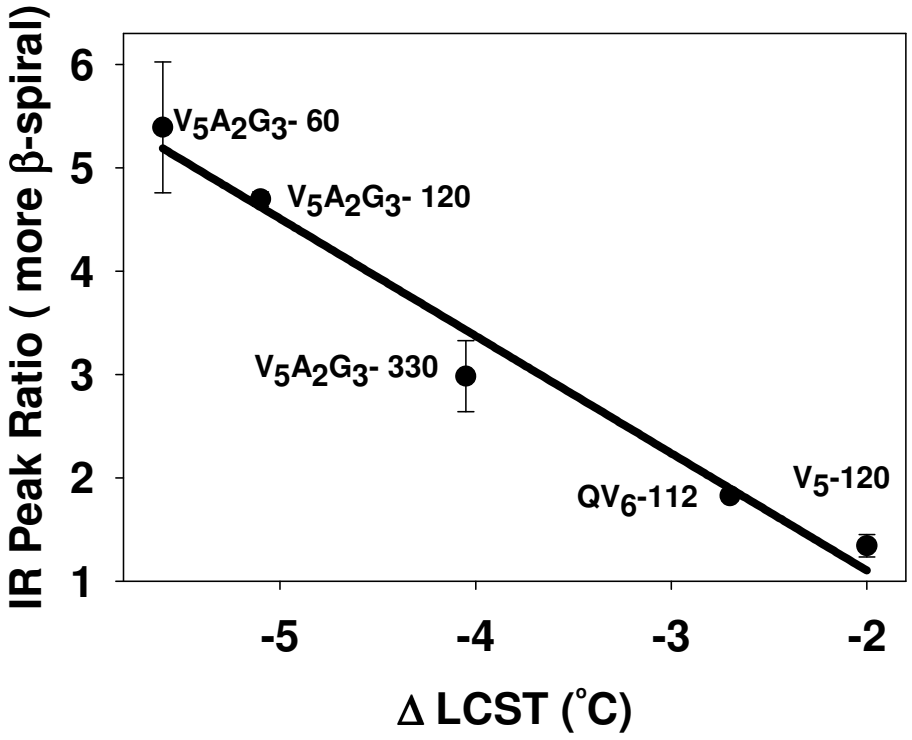

Figure 4.5. Plot of the IR peak area ratio of (1619+1663 cm^{-1})/ (1642 cm^{-1}) vs. Δ LCST for the five ELPs.

Enthalpic Contribution of b-spiral Formation by DSC

Finally, differential scanning calorimetry (DSC) measurements were carried out with all five ELP's in D_2O and H_2O (Table 4.2). The hydrophobic collapse of the ELPs was found to be endothermic in all cases in both solvents (Figure 4.6). This unfavorable enthalpic change upon going from H_2O to D_2O was smaller for the less hydrophobic ELPs and directly correlated with the change in the LCST value (Figure 4.7). Therefore, the LCST change in D_2O vs. H_2O can be directly tied to the enthalpic gain from β-spiral formation (Figures 4.5 & 4.7).

It should be noted that the free energy of the phase transition for ELPs is expected to be negative on entropic grounds.[39] Indeed, as the polypeptide chains collapse and aggregate, bound solvent molecules are released into the bulk solution. This positive entropic change is widely thought to be the central driving force of the hydrophobic collapse of ELPs.[49] Since the enthalpic cost of undergoing hydrophobic collapse increases the least for the least hydrophobic ELPs in D_2O, the free energy gain for these systems is correspondingly larger, By contrast with ELPs, PNIPAM displays a higher enthalpic cost for undergoing its phase transition in D_2O compared to H_2O.[50] This is not surprising, since far few hydrogen bonds are formed upon the collapse of PNIPAM.

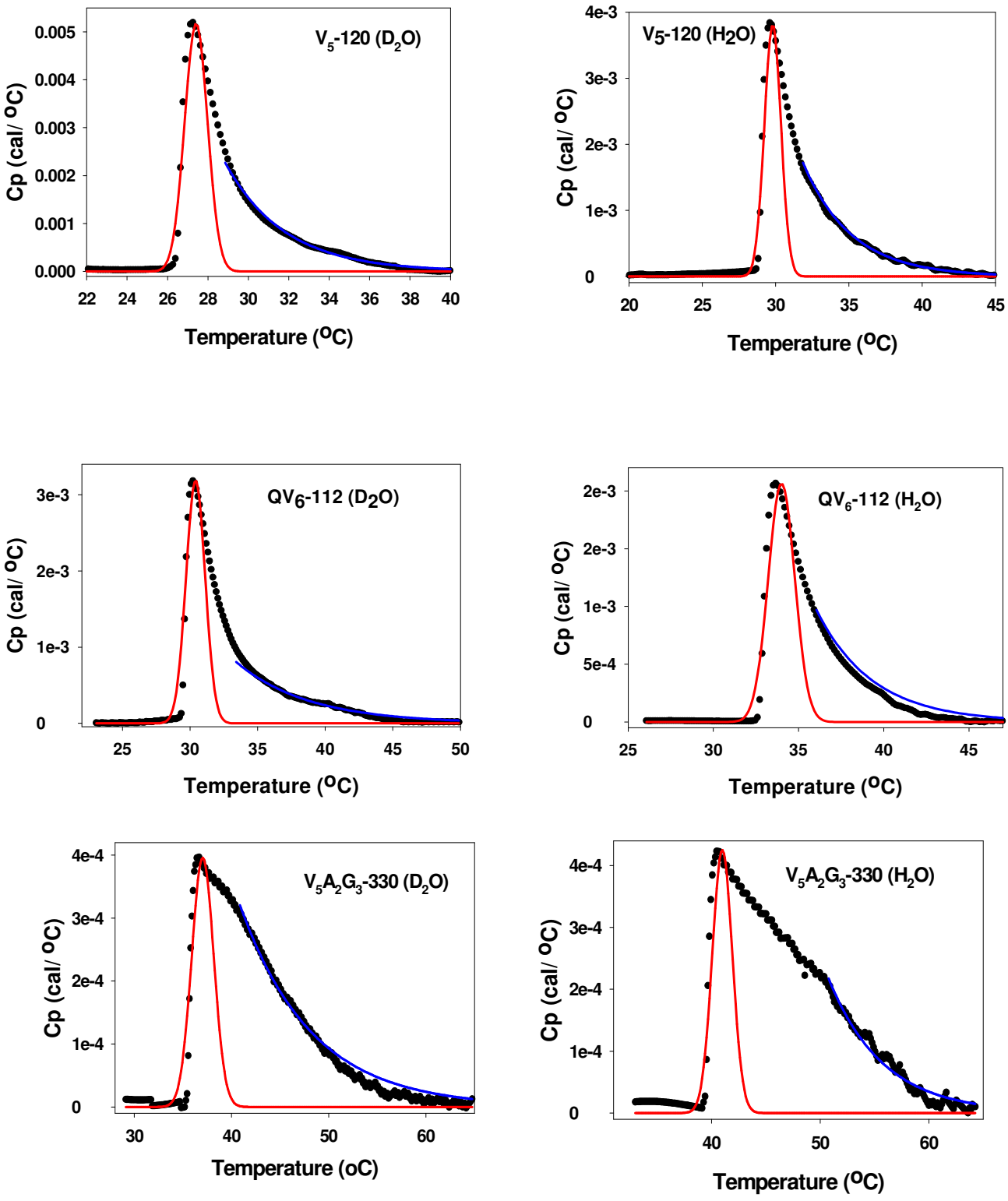

Figure 4.6. DSC data of five ELPs in H_2O and D_2O. Black dotted line is original data, red line is the fit to Gaussian, blue is the fit to exponential.

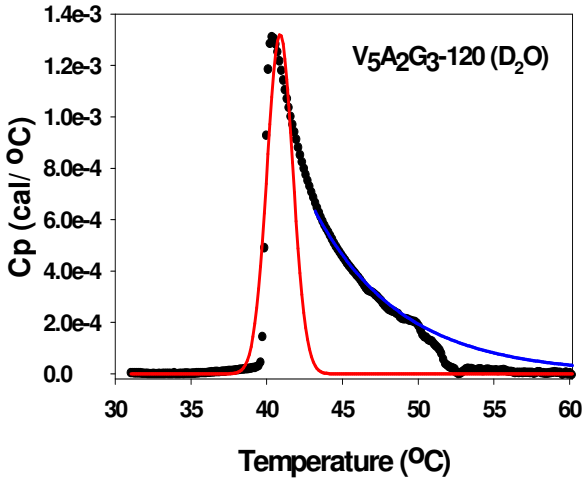

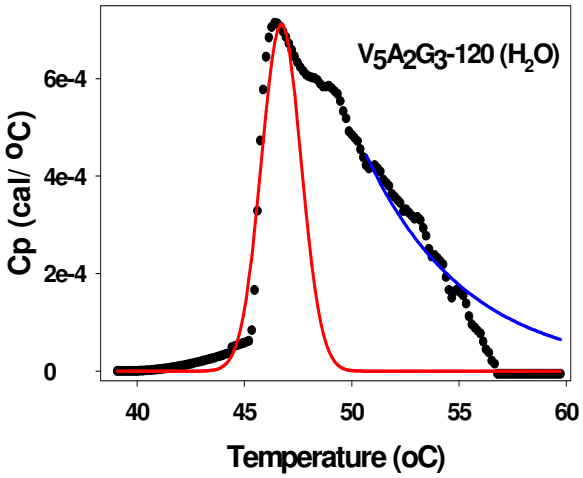

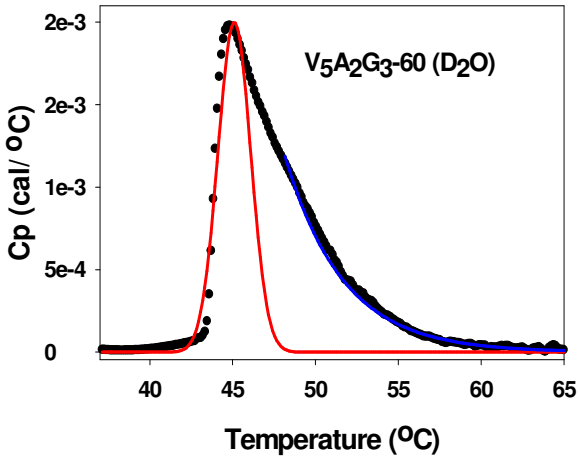

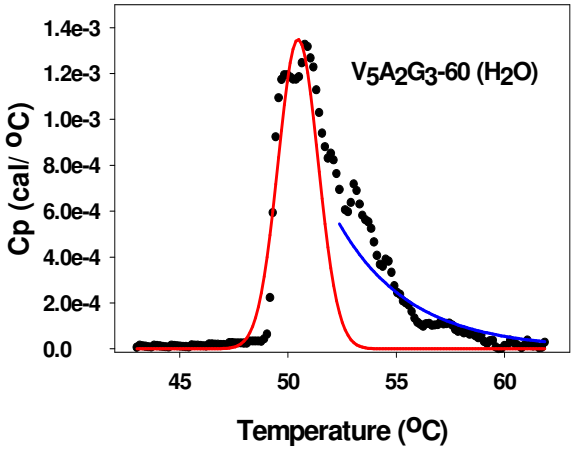

Figure 4.6. Continued

Table 4.2: ΔH of ELPs in D_2O and H_2O (ΔH is area under the Gaussian from the DSC data) $\Delta\Delta H_{DH}$ = ΔH D_2O- ΔH H_2O.

	ΔH H_2O (kcal/mol)	**ΔH D_2O (kcal/mol)**	**$\Delta\Delta H_{DH}$ (kcal/mol)**
V_5-120	631.5	962.30	330.7
QV_6-112	510.7	760	249.2
$V_5A_2G_3$-330	325.5	525.2	199.7
$V_5A_2G_3$-120	213.8	341.5	127.7
$V_5A_2G_3$-60	172.5	251.0	78.4

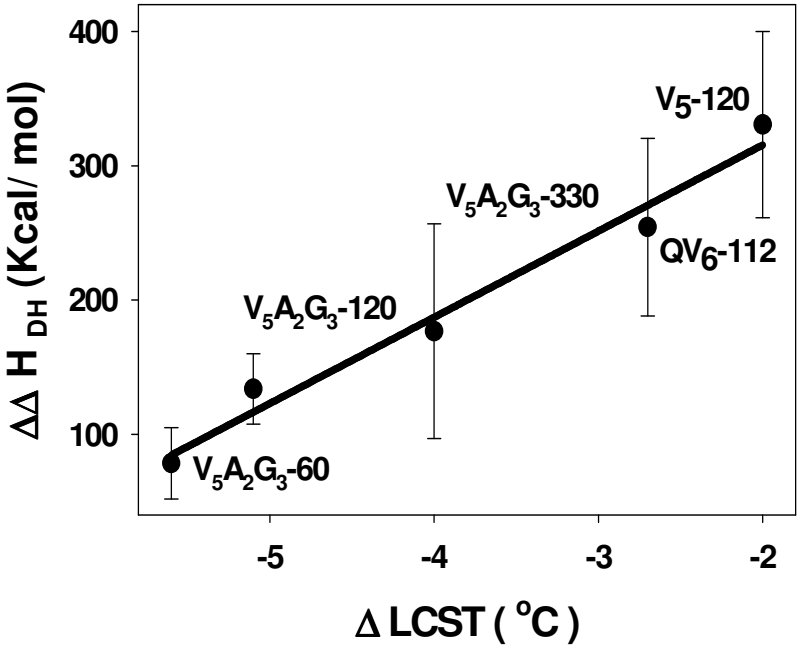

Figure 4.7. Correlation plot of IR peak ratio vs. ΔΔH from ELPs in D_2O solution to H_2O solution.

From the data shown here, it is clear that hydrophobic effects are not the dominant factor for the stabilization of elastin-like polypeptides in D_2O. Instead, hydrogen bonding involved in structure formation is shown to be the key factor in the stabilization of elastin-like polypeptides in D_2O. Moreover, β-spiral structure is preferentially stabilized over random coil structure in D_2O. Finally, we note that the ELPs measured here are largely neutral with very few amino acids with charged or polar side chains (< 3% of all residues). Such polar residues may play a role in protein stabilization in D_2O for certain proteins. Therefore, future studies will need to include isotopic effects on the LCST of ELPs with increasing amounts of such residues.

CHAPTER V

THERMORESPONSIVE POLYPEPTIDE CONJUGATED SOLID SUPPORTED LIPID BILAYER AS A BIOSENSOR

Introduction

Development of devices that can achieve selective and sensitive sensing of analytes is an important but difficult problem in chemical, biological, and pharmaceutical research. Microfluidic devices are one of the most widely used biosensor platforms due their multiplexing analysis capability and relatively easy and affordable fabrication process. In addition to this, it requires only a small volume of sample which can be extremely beneficial in detection of trace amount of analytes.

Solid supported lipid bilayer is one of the most widely used in situ cell mimic system. In solid supported lipid bilayer system, two dimensional fluidity of the lipid bilayer is preserved by a water layer in between the solid substrate and the bilayer. [51] Incorporation of fluid lipid membranes with microfluidic device has been shown promises as a powerful ligand- receptor interaction biosensing platform .[52,53]

In this study, the thermoresponsive polypeptide ELP is tethered to a lipid bilayer and employed as a size selective filter. ELPs undergo a phase transition and the temperature where the phase transition occurs is referred as lower critical solution temperature (LCST). The LCST of ELPs can be influenced by their amino acid composition, chain length, temperature, salt concentrations, pH, and pressure. ELPs consist of pentameric repeat unit of (ValProGlyXGly) where X can be any amino acids

but proline. The chemical properties of ELP can be precisely controlled by substituting different amino acids in the guest residue position or altering the number of repeat units. ELPs employed in this study are ELP V_5-120 and ELP $V_5A_2G_3$-120. The major advantage of using ELP as a filter in the biosensor is its phase transition property. Unlike the PEG system where the polymer's conformation can be altered only by changing the polymer density on the surface, the conformation of ELP can be altered from an extended state to a collapsed state on the same sample device. The sensing capability of ELP-conjugated lipid biosensor can be on or off on the same sample device by increasing salt concentration or temperature. Here we show modulation in binding of antibody IgG to biotin on the surface of lipid bilayer by changing the ELP's conformation state by salt (Figure 5.1).

Experimental

Materials

1-Palmitoyl-2-Oleoyl-*sn*-Glycero-3-Phosphocholine (POPC), 1,2-Dipalmitoyl-*sn*-Glycero-3-Phosphoethanolamine-N-(Glutaryl) (Sodium Salt), and 1,2-Dipalmitoyl-*sn*-Glycero-3-Phosphoethanolamine-N-(Cap Biotinyl) (Sodium Salt) were purchased from Avanti Polar Lipids (Alabaster, AL). Texas Red-DHPE and rabbit IgG antibodies were purchased from Invitrogen, Inc. (Carlsbad, California). The rabbit IgG was labeled with Alexa Fluor-594 dye by using a standard protein-labeling kit (A10239, Invitrogen, Carlsbad, California). Labeling degree was determined as numbers of fluorophores per protein by UV/vis absorption spectroscopy. The dye-labeled IgG was stored in a 10 mM

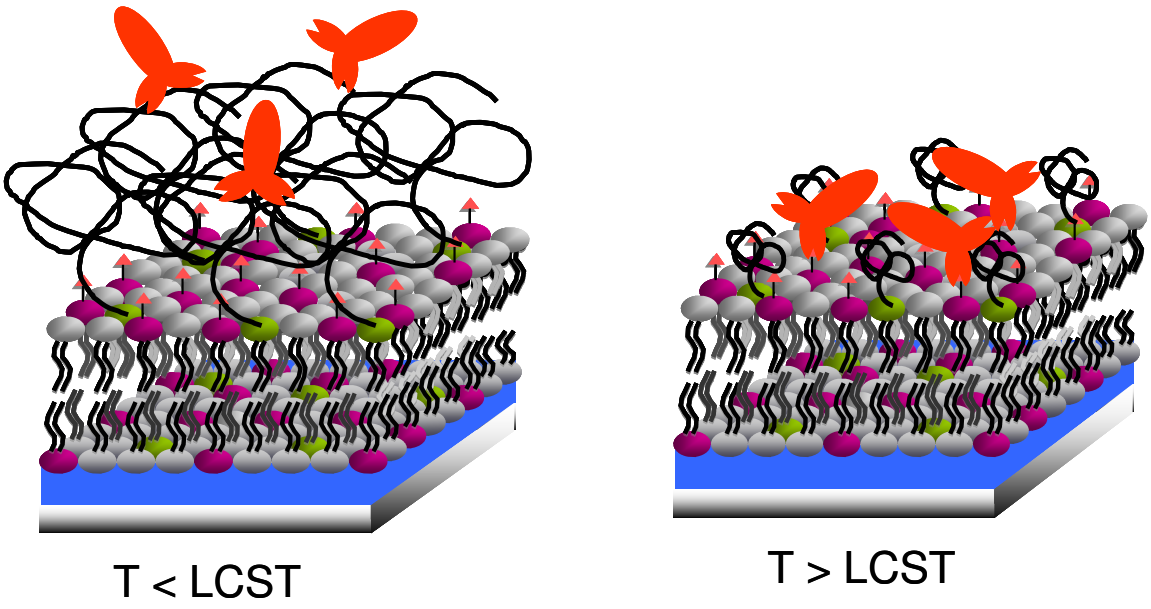

Figure 5.1. Schematic diagram of ELP conjugated lipid bilayer on a glass substrate. When temperature is below LCST of the corresponding ELP, protein is block by extended ELP chain (left). When temperature is above its LCST, ELP chain collapses then protein is more accessible to the ligand on the surface of bilayer.

sodium phosphate buffer solution at pH 6.9 made with purified water from a NANOpure Ultrapure Water System (18.2 MΩcm, Barnstead, Dubuque, IA).

Microfluidic Device Fabrication

All the binding experiments were done in microfluidics devices. The device consists of PDMS mold attached on a borosilicate substrate. The five-channel microfluidic devices were fabricated by soft lithographic techniques as previously described. First, Corel Draw software (Version 9, Corel Corp.) was used to draw a pattern of five channel microfluidics then the design is transferred onto black and white high-contrast Kodak technical pan film. The patterned film is used as a photomask for photolithography. The preparation of glass slides was as follow. Soda-lime glass slides were immersed in a diluted surfactant solution (ICN x 7 detergent, Costa Mesa, CA) and boiled for an hour. The glass slides were rinsed with purified water and dried with nitrogen gas. The cleaned glasses were spin-coated with a thin layer of hexamethyldisilazane (HMDS) to improve adhesion of the photoresist to the glass surface followed by spin coating with Shipley 1827 photoresist at 1000 rpm for 20 seconds. The photomask was placed on the photoresist treated glass substrate then exposed to UV light with Quintel Q4000 Mask Aligner and treated with developing solution. The substrate is baked at 120 ^{o}C overnight before the glass etching procedure.

The substrates were alternatively immersed in buffered oxide etchant contains HF and 1 M HCl solution until the photoresist pattern on the glass started to stripe away. After etching, the remaining photoresist was removed with ethanol and dried. PDMS was then poured over the glass masters and cured in an oven at 55 ^{o}C for 3-5 hrs. The

inlets and outlets were created on the PDMS before a galss substrate is attached. Borosilicate substrates were cleaned had in a boiling diluted solution of ICN x7 detergent. Then the substrates were rinsed with purified water, dried with nitrogen, and annealed in a kiln at 480 °C for 5 h before introduction into the oxygen plasma. The PMDS molds and cleaned borosilicate glass substrates were treated in oxygen plasma for 20 s. Finally, the PDMS molds and glass substrates were brought into contact immediately after oxygen plasma treatment to create finished microfluidic devices.

Solid Supported Bilayer Formation with Small Unilarmella Vesicles

Preparation of SUV were done by vesicle extrusion as previously described.[54, 55] First, lipids in chloroform were mixed to a desired ratio and majority of the chroloform was evaporated under a stream of nitrogen. Further evaporation of chloroform was done by placing the lipid mixture under a vacuum for 3-4 hrs. Dried lipid mixture was rehydrated with 10 mM phosphate buffer at pH 6.9 followed by 10 cycles of freeze/ thaw. After the freeze/ thaw, vesicle solutions were extruded 5 times with 100 nm polycarbonate filter (Whatman) then 5 times with 50 nm filter. The vesicle size after the extrusion was examined to be ~90 nm by dynamic light scattering with Brookhaven Instruments 90Plus Particle Size Analyzer.

Prepared SUV solution was introduced into a PDMS microfluidics device by simply injecting the solution through an inlet port. The introduction of lipid solution to the PMDS device was done immediately after plasma treatment and bonding of the PDMS/glass microfluidic platform to ensure that the surfaces remained hydrophilic. The

fusion of lipid vesicles on the glass surface inside the PDMS device is done within 15 min.

In case of highly charged vesicles with more than 10 mol% of charged lipids, however, requires ionic solution to form a mobile bilayer. The microchannels were rinsed with water after 15 min of incubation in order to remove the excess lipid solution from the channels.

Fluorescence Recovery After Photobleaching (FRAP)

The quality and mobility of supported lipid bilayers was examined by FRAP using an inverted epifluorescence Nikon Eclipse TE2000-U microscope. Once bilayer is formed on a glass substrate, the sample is exposed to a laser radiation from a 2.5 W mixed gas Ar^+/Kr^+ laser (Stabilite 2018, Spectra Physics) and a bleached spot of ~ 17 μm full width at half maximum is generated with 10X objective. The fluorescence recovery at the bleached spot was obtained with a MicroMax 1024b CCD camera (Princeton Instruments) and recorded every 10 seconds for 10 minutes as time lapse images with Metamorph Software. The fluorescence intensity of the bleached spot was then determined as a function of time after background subtraction and intensity normalization. A fluorescence recovery curve was fit to the following equation:

$$D = \frac{\omega}{4\tau_{1/2} + \gamma_D} \tag{5.1}$$

D is the diffusion constant, $\tau_{½}$ is the half time of recovery, ω is the full width at half-maximum of the Gaussian profile of the focused beam and rd is a correction factor that

depends on the bleach time and geometry of the laser beam. Herein, ω = 17.0 μM, and the value of γ_D was 1.2

ELP- Bilayer Conjugation

ELPs used in this study are expressed in E.*coli* and purified as described previously in Chapter II. In situ conjugation of ELPs to the top layer of lipid bilayer is done by 1-Ethyl-3-(3-dimethylaminopropyl)-carbodiimide (EDC) and N-Hydroxysuccinimide (NHS) coupling reaction. Chemical structures of EDC and NHS are as shown in Figure 5.2. Carboxylic groups on the Glutaryl PE react with EDC/ NHS to form a semi-stable amine-reactive NHS-ester by incubating with 0.2 M EDC/ 0.3 M NHS solution for 15 min. Then 1 mg/ mL ELP solution is flowed inside the channels and incubated for one hour. The amine groups on the ELP's N-terminal forms a stable amide bond with the lipid head groups during the incubation.

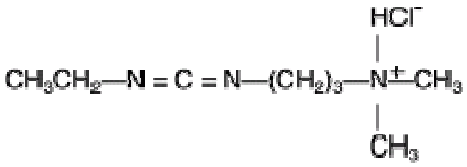

Ethyl-3-(3-dimethylaminopropyl)-carbodiimide (EDC)

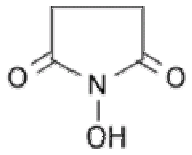

N-Hydroxysuccinimide (NHS)

Figure 5.2. Chemical structure of EDC and NHS.

Total Internal Reflection Fluorescence Microscopy

Binding of fluorescence labeled antibody IgG to the biotins on the surface of lipid bilayer is measured by total internal reflection fluorescence microscopy (TIRFM). TIRFM is used to detect fluorescence signals mostly from the surface rather than the bulk. The TIRFM images were taken followed by the previously described methods. [52,55, 57] Various concentrations of Alexa 594-labeled rabbit IgG solutions were flowed through each channel until the epi fluorescence signal was saturated. The fluorescence images were obtained with a Nikon E800 fluorescence microscope using a 4X objective. A 594-nm helium-neon laser beam (4 mW, Uniphase, Manteca, CA) was passed through a line generator lens (BK7 for 30°, Edmund Optics, Barrington, NJ) to create a uniform intensity profile across the microchannel array. The helium-neon laser beam was then passed through a dove prism. Drop of an index matching immersion oil was placed on the top of the dove prism to optically couple the borosilicate substrate of the microfluidics device. As the laser illuminated the interface between the bilayer-coated glass substrate and the bulk aqueous solution, it was totally internally reflected, creating an evanescent wave above the interface. The evanescent wave decayed exponentially to its 1/e value by ~70 nm above the interface under the experiment conditions employed here. This allowed the proteins bound to the supported lipid bilayer to be studied with high specificity. The TIRFM images were captured with a Micromax 1024b CCD camera, collected using Metamorph software (Universal Imaging Corp.), and transferred to Sigma Plot for further processing. Measurements of thermodynamic binding constants were made only after the fluorescence intensity from the interface reached equilibrium.

Results and Discussion

ELP conjugated lipid bilayers were examined by FRAP to insure the quality and the mobility of the system. A FRAP curve and a fluorescence microscope image of ELP $V_5A_2G_3$-120 conjugated bilayer with 5 mol % Glutaryl PE, 10 mol % Biotinyl PE, and 0.1 mol % Texas Red DHPE in POPC is shown in Figure 5.3. As can be seen in the Figure below, the quality and mobility of the bilayer was preserved after an in situ ELP conjugation.

Binding of IgG-biotin experiments with varying biotin density on the surface was done to find a saturation concentration of biotin for IgG. Experiments are done in a seven channel microfluidic device. In each channel, lipid bilayer contains varying concentration of biotinyl-PE is formed then the same concentration of fluorescence labeled antibody IgG is introduced. The TIRFM image of the sample is as shown in Figure 5.4. From the left to the right, the lipid bilayers contain 0, 0.5, 2, 10, 15, 20, and another 20 mol % biotinyl-PE. From the data, we can assume that antibody IgG reached the maximum binding capacity on the surface with 10 mol% biotin.

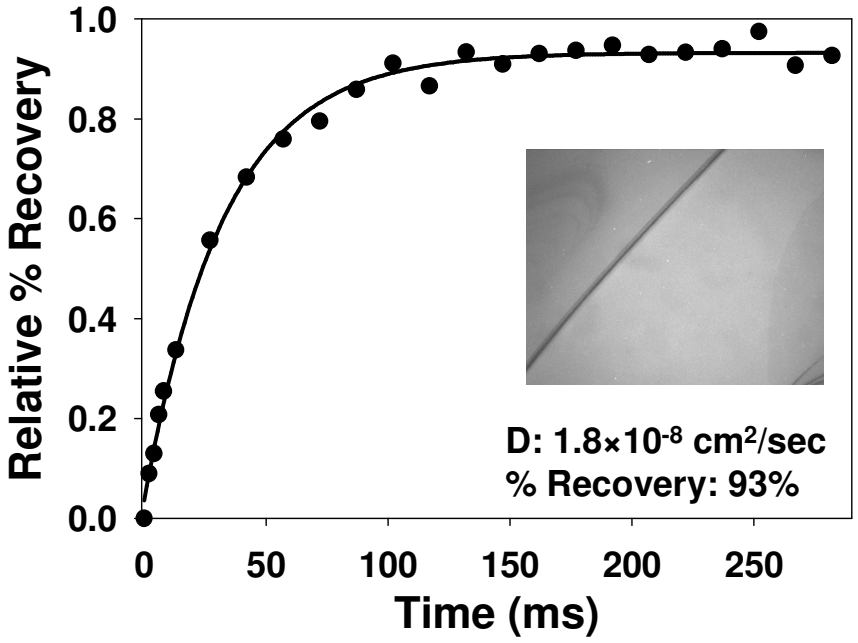

Figure 5.3. FRAP curves from ELP $V_5A_2G_3$-120 conjugated bilayers on planar borosilicate substrates: recovery curve for a membrane containing 5 mol % Glutaryl PE, 10 mol % Biotinyl PE, and 0.1 mol % Texas Red DHPE in POPC. Inset: fluorescence microscope image of the same ELP $V_5A_2G_3$-120 conjugated bilayer.

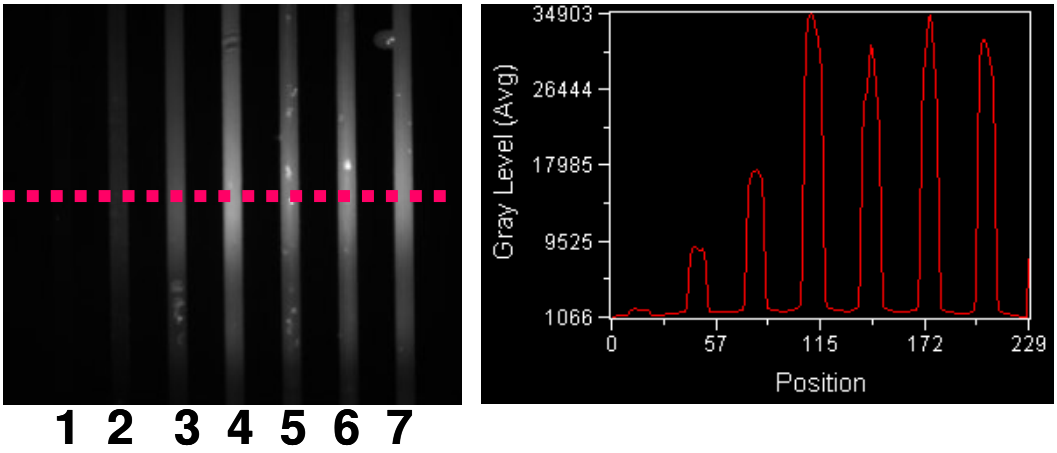

Figure 5.4. (Left) TIRFM image of antibody IgG binding assay with six different biotin PE concentrations in the bilayers. Red dotted line represents the line scan. Right: line scans profile from the red dotted region of TIRFM image.

Next we created lipid bilayer inside the five channel microfluidics. In channel (1), (4), and (5) lipid bilayers containing 1 mol% biotinyl PE was created. In channel (2) and (3), 9 mol% biotinyl PE is incorporated. Concentration of glutaryl PE is 0.5 mol% in all channels and POPC was used as a background lipid. Once stable bilayer is formed, 0.2 M EDC/ 0.3 M NHS solution was flowed inside channels 2 through 5 for an activation of carboxyl group on the Glutaryl-PE head group. After treating 15 min incubation of bilayer with EDC/ NHS solution, 1 mg/mL ELP $V_5A_2G_3$-120 solution was introduced for ELP- lipid conjugation. In channel (2) and (4), 0.4 M Na_2SO_4 solution was introduced to induce the phase transition of ELPs. Finally, 1 mg/mL dye labeled antibody IgG, was introduced in all channels. It should be noted that channels which ion solution was flowed previously, same concentration of Na_2SO_4 was added to the antibody IgG solution in order to keep the ELP chains in the same phase upon the introduction of the protein solution. it should be mentions that we also did a control experiment to show 0.5 M Na_2SO_4 doesn't effects the binding of IgG to biotin.

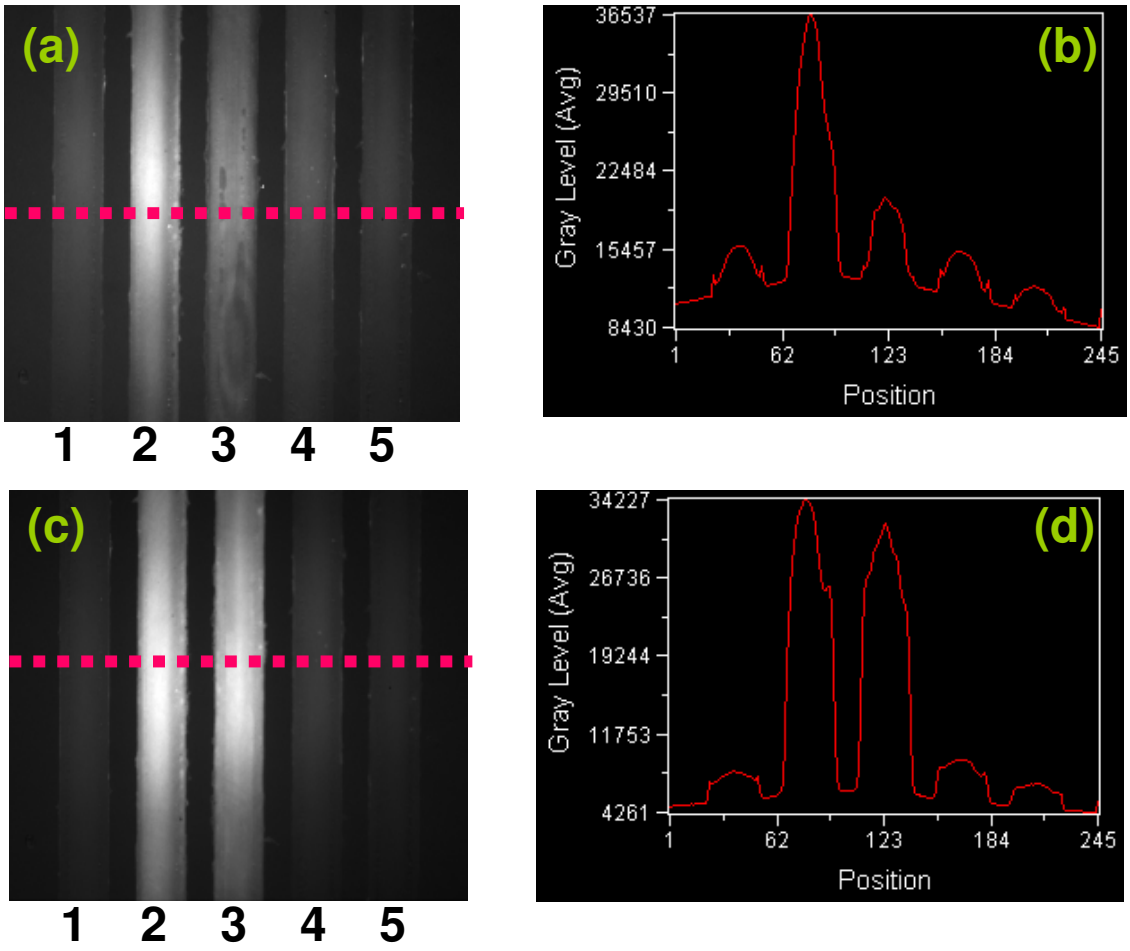

Figure 5.5. (a)TIRFM image of ELP $V_5A_2G_3$-120 conjugated lipid bilayer sensor. Fluorescence signal is from Alexa 594 labeled antibody IgG bound to the biotin on the surface on bilayer. (b) Line scan of the red dotted region in image (a). (c) TIRFM image of the same sample as (a) after flow an IgG solution without salts in the channel (3). (d) line scan of the red dotted region in image (c).

As it can be seen from the Figure 5.5, the fluorescence intensity of channel (3) is about 1/3 of the fluorescence intensity of (2). This is due to the change in accessibility of antibody IgG depending on the conformational state of ELP chains on the surface. In case of channel (2) where the ELP chains are in its extended state, the antibody IgG molecules are blocked by the ELP chains. On the other hand, when ELP chains are in the collapsed state as in case of channel (3), the antibody IgG get relatively easier access to the biotin on the surface of lipid bilayers.

Next, we employed ELP V_5-120 which is more hydrophobic than ELP V5A2G3-120 with lower LCST. In this experiment, we hypothesized if there would be an increase in selectivity with more biotin on the surface of the lipid bilayers. In five channel microfluidics, lipid samples containing 20 mol% Biotinyl-PE, 0.5 mol% Glutaryl-PE, and 0.1 mol% Texas Red DHPE in POPC fused. Once stable supported lipid bilayer is formed, EDC/ NHS coupling of the ELP to the bilayer is done in all the channels. In channels (1), (3) and (5) 0.5 M Na2SO4 solution was flowed in order to induce the phase transition of the ELP. Finally, dye labeled antibody IgG with/or without salt was introduced. The antibody solution was flowed until there was no change in fluorescence level by epi fluorescence microscopy. Once the saturation level of fluorescence was observed, a TIRFM image of the sample was taken. As it can be seen in Figure 5.6., the fluorescence level in the channels (1), (3), (5) and (2), (4) was significantly different. Interestingly, the fluorescence intensity level of (1), (3), (5) was recovered after rinsing the channels with water and flowed the IgG solution without salt. This result strongly

supports out theory that extended states of ELP block the antibody from getting to the surface but once ELP is collapsed, the antibody have an easier access to the surface.

This study demonstrates a capability of employing elastin-like polypeptides conjugated bilayer as an on/off size dependent sensor using a micro fluidic platform. The selectivity of the sensor was up to 7:1 difference in binding of antibody IgG with 20 mol% biotin on the surface. Further control experiments will be needed in order to confirm the current theory.

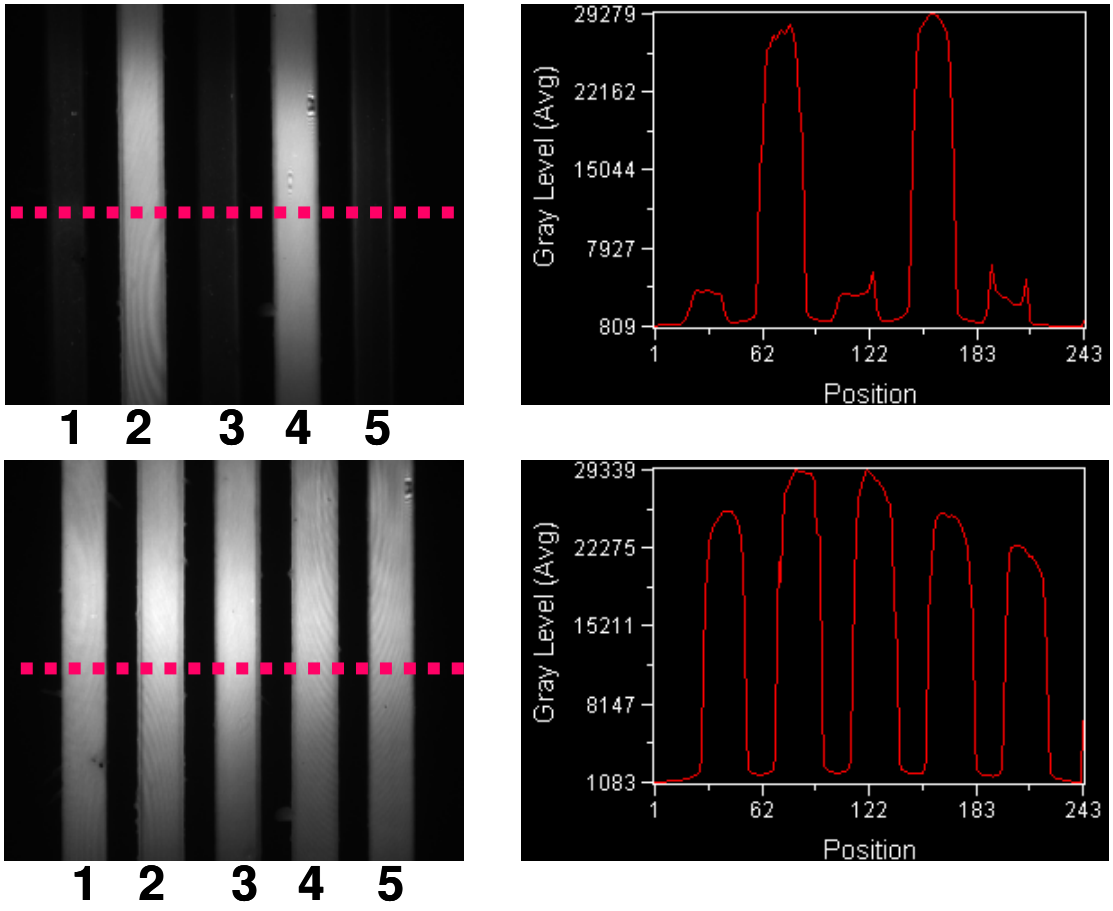

Figure 5.6. (top left)TIRFM image of ELP V_5-120 conjugated lipid bilayer sensor. Fluorescence signal is from Alexa 594 labeled antibody IgG bound to the biotin on the surface on bilayer. (top right) Line scan of the red dotted region in image (top left). (bottem left) TIRFM image of the same sample as (top left) after flow an IgG solution without salts in the channel (1), (3), and (5) (d) line scan of the red dotted region in image (c).

CHAPTER VI

CONCLUSIONS

Elastin-like polypeptides are simple and powerful model system to study various properties of chemistry. It is also widely used thermoresponsive materials in bio-inspired application. By using ELPs as model system, we successfully achieved a better understanding of thermodynamics of specific anion effects and solvent isotope effects and also potential use of ELP as a part of bio sensing device.

First, specific anion effects on phase transition temperature of neutral and positively charged ELPs shed a light on molecular level understanding of Hofmeister effects on stability of biomacromolecules. The phase transition temperature of two neutral ELPs followed a general direct Hofmeister series. Salting- out effects of kosmotropic anions are based on their ability to polarize the water molecules that are specifically hydrogen bonded to the polypeptides. Chaotropic anions salt-out peptides through a surface tension increment mechanism. Surface tension around the exposed hydrophobic moieties on ELPs increases upon the addition of chaotropic anions. Chaotropic anions also exhibit a non-linear binding behavior at low salt concentration which is due the direct binding of anions to the polypeptide chains. The phase transition temperature of positively charged ELP showed both inverse and direct Hofmeister series. The LCST vs. salt concentration plot of ELP KV_6-112 showed an exponential drop of LCST at low salt concentration regime (below 100 mM) due to the charge screening effects of anions. at the high salt concentration region, the LCST vs. salt concentration data shows a direct Hofmeister series. Once the overall positive charge on

the polypeptide is neutralized, anion effects on the LCST are based on their ability to increase the surface tension around polypeptides.

Next, we investigated solvent isotope effects on phase transition temperature of various neutral ELPs. The LCST of five neutral ELPs, ELP V_5-120, ELP QV_6-112, ELP $V_5A_2G_3$-330, ELP $V_5A_2G_3$-120, and ELP $V_5A_2G_3$-60 were measured in light and heavy water. Secondary structure of the ELPs was quantified by FTIR, and CD and change in enthalpy upon hydrophobic collapse were measured by DSC. The data strongly suggest that the hydrogen bonding is an important factor in stabilization of the ELP. The results of this study imply that the hydrogen bonding can be a major factor in stability of biomacromolecules rather than hydrophobicity.

ELP was also incorporated as a part of a binding sensor device. ELP conjugated bilayer was formed inside a microfluidic device. The binding of antibody to the ligand on the surface of bilayer was modulated by changing the conformation of ELP on the surface up to 7:1 difference.

REFERENCES

(1) Baldwin, R. L. *Biophys. J.* **1996**, *71*, 2056.

(2) Collins, K. D.; Washabaugh, M. W. *Q. Rev. Biophys.* **1985**, *18*, 323; Hofmeister, F. *Arch. Exp. Pathol. Pharmakol* **1888**, *24*, 247; Kunz, W.; Henle, J.; Ninham, B. W.*Curr. Opin. Colloid Interface Sci* **2004**, *9*, 19.

(3) Kunz, W.; Lo Nostro, P.; Ninham, B. W. *Curr. Opin. Colloid Interface Sci.* **2004**, *9*, 1.

(4) Bostrom, M.; Williams, D. R. M.; Ninham, B. W. *Langmuir* **2002**, *18*, 6010; Craig, V. S. J. *Curr. Opin. Colloid Interface Sci.* **2004**, *9*, 178; Salis, A.; Pinna, M. C.; Bilanicova, D.; Monduzzi, M.; Lo Nostro, P.; Ninham, B. W. *J. Phys. Chem. B* **2006**, *110*, 2949; Dexter, A. F. *J. Phys. Chem. B* **2005**, *109*, 14750; Evans, D. F.; Mitchell, D. J.; Ninham, B. W. *J. Phys. Chem.* **1984**, *88*, 6344.

(5) Batchelor, J. D.; Olteanu, A.; Tripathy, A.; Pielak, G. J. *J. Am. Chem. Soc.* **2004**, *126*, 1958.

(6) Gurau, M. C.; Lim, S. M.; Castellana, E. T.; Albertorio, F.; Kataoka, S.; Cremer, P. S. *J. Am. Chem. Soc.* **2004**, *126*, 10522.

(7) Omta, A. W.; Kropman, M. F.; Woutersen, S.; Bakker, H. J. *Science* **2003**, *301*, 347; Omta, A. W.; Kropman, M. F.; Woutersen, S.; Bakker, H. J. *J. Chem. Phys.* **2003**, *119*, 12457.

(8) Smith, J. D.; Saykally, R. J.; Geissler, P. L. *J. Am. Chem. Soc.* **2007**, *129*, 13847.

(9) Collins, K. D.; Neilson, G. W.; Enderby, J. E. *Biophys. Chem.* **2007**, *128*, 95.

(10) Vonhippe.Ph; Peticola.V; Schack, L.; Karlson, L. *Biochemistry* **1973**, *12*, 1256.

(11) Vonhippe.Ph; Schleich, T. *Acc. Chem. Res.* **1969**, *2*, 257.

(12) P.H., V.; Wong, K. Y. *Science* **1964**, *145*, 577; Song, J. D.; Ryoo, R.; Jhon, M. S. *Macromolecules* **1991**, *24*, 1727.

(13) Ninham, B. W.; Yaminsky, V. *Langmuir* **1997**, *13*, 2097.

(14) Bostrom, M.; Williams, D. R. M.; Ninham, B. W. *Phys. Rev. Lett.* **2001**, *8716*; Nandi, P. K.; Robinson, D. R. *J. Am. Chem. Soc.* **1972**, *94*, 1299; Schellman, J. A. *Biophys. J.* **2003**, *85*, 108; Pegram, L. M.; Record, M. T. *J. Phys. Chem. B* **2007**, *111*, 5411.

(15) Pegram, L. M.; Record, M. T. *Proc. Nat. Acad. Sci. U.S.A.* **2006**, *103*, 14278.

(16) Zhang, Y. J.; Furyk, S.; Bergbreiter, D. E.; Cremer, P. S. *J. Am. Chem. Soc.* **2005**, *127*, 14505.

(17) Tiktopulo, E. I. U., V.N.;Lushchik, V.B.; Klenin, S.I.; Bychkova, V.E.; Ptitsyn, O.B. *Macromolecules* **1995**, *28*, 7519.

(18) Meyer, D. E.; Chilkoti, A. *Biomacromolecules* **2002**, *3*, 357.

(19) Meyer, D. E.; Chilkoti, A. *Biomacromolecules* **2004**, *5*, 846.

(20) Meyer, D. E.; Trabbic-Carlson, K.; Chilkoti, A. *Biotechnol. Progr.* **2001**, *17*, 720 ; Nath, N.; Chilkoti, A. *J. Am. Chem. Soc.* **2001**, *123*, 8197; Trabbic-Carlson, K.; Meyer, D. E.; Liu, L.; Piervincenzi, R.; Nath, N.; LaBean, T.; Chilkoti, A. *Protein Eng. Des. Sel.* **2004**, *17*, 57; Urry, D. W.; Luan, C. H.; Parker, T. M.; Gowda, D. C.; Prasad, K. U.; Reid, M. C.; Safavy, A. *J. Am. Chem. Soc.* **1991**, *113*, 4346; Meyer, D. E.; Chilkoti, A. *Nat. Biotechnol.* **1999**, *17*, 1112.

(21) Yamaoka, T.; Tamura, T.; Seto, Y.; Tada, T.; Kunugi, S.; Tirrell, D. A. *Biomacromolecules* **2003**, *4*, 1680.

(22) Reguera, J.; Urry, D. W.; Parker, T. M.; McPherson, D. T.; Rodriguez-Cabello, J. C. *Biomacromolecules* **2007**, *8*, 354.

(23) Flamia, R.; Zhdan, P. A.; Martino, M.; Castle, J. E.; Tamburro, A. M. *Biomacromolecules* **2004**, *5*, 1511; Ohgo, K.; Ashida, J.; Kumashiro, K. K.; Asakura, T. *Macromolecules* **2005**, *38*, 6038; Kumashiro, K. K.; Kurano, T. L.; Niemczura, W. P.; Martino, M.; Tamburro, A. M.*Biopolymers* **2003**, *70*, 221; Ohgo, K.; Kurano, T. L.; Kumashiro, K. K.; Asakura, T. *Biomacromolecules* **2004**, *5*, 744; Yao, X. L.; Hong, M. *J. Am. Chem. Soc.* **2004**, *126*, 4199; Schmidt, P.; Dybal, J.; Rodriguez-Cabello, J. C.; Reboto, V. *Biomacromolecules* **2005**, *6*, 697; Bostrom, M.; Williams, D. R. M.; Ninham, B. W. *Phys. Rev, Lett.* **2001**, *8716*.

(24) Mao, H. B.; Holden, M. A.; You, M.; Cremer, P. S. *Anal. Chem.* **2002**, *74*, 5071; Mao, H. B.; Li, C. M.; Zhang, Y. J.; Bergbreiter, D. E.; Cremer, P. S. *J. Am. Chem. Soc.* **2003**, *125*, 2850; Mao, H. B.; Yang, T. L.; Cremer, P. S. *J. Am. Chem. Soc.* **2002**, *124*, 4432.

(25) Zhang, Y.; Furyk, S.; Sagle, L. B.; Cho, Y.; Bergbreiter, D. E.; Cremer, P. S. *J. Phys. Chem. C* **2007**, *111*, 8916.

(26) Zhang, Y. J.; Mao, H. B.; Cremer, P. S. *J. Am. Chem. Soc.* **2003**, *125*, 15630.

(27) Marcus, Y. *Ion Properties*; Marcel Dekker, 1997.

(28) Jarvis, N. L.; Scheiman, M. A. *J. Phys. Chem.* **1968**, *72*, 74.

(29) Jungwirth, P.; Tobias, D. J. *Chem. Rev.* **2006**, *106*, 1259.

(30) Chen, X.; Yang, T.; Kataoka, S.; Cremer, P. S. *J. Am. Chem. Soc.* **2007**, *129*, 12272.

(31) Rice, C. V. *Biomacromolecules* **2006**, *7*, 2923-2925.

(32) Leunissen, M. E.; van Blaaderen, A.; Hollingsworth, A. D.; Sullivan, M. T.; Chaikin, P. M. *Proc. Nat. Acad. Sci. U.S.A.* **2007**, *104*, 2585.

(33) Meyer, D. E.; Trabbic-Carlson, K.; Chilkoti, A. *Biotechnol. Progr.* **2001**, *17*, 720; Nath, N.; Chilkoti, A. *J. Am. Chem. Soc.* **2001**, *123*, 8197; Urry, D. W.; Luan, C. H.; Parker, T. M.; Gowda, D. C.; Prasad, K. U.; Reid, M. C.; Safavy, A. *J. Am. Chem. Soc.* **1991**, *113*, 4346.

(34) Cho, Y.; Zhang, Y. J.; Christensen, T.; Sagle, L. B.; Chilkoti, A.; Cremer, P. S. *J. Phys. Chem. B* **2008**, *112*, 13765.

(35) Boström, M.; Tavares, F. W.; Finet, S.; Skouri-Panet, F.; Tardieu, A.; Ninham, B. W. *Biophys Chem* **2005**, *117*, 217; Finet, S.; Skouri-Panet, F.; Casselyn, M.; Bonnete, F.; Tardieu, A. *Curr. Opin. Colloid Interface Sci.* **2004**, *9*, 112.

(36) Pegram, L. M.; Record, M. T. *J. Phys. Chem. B* **2007**, *111*, 5411; Pegram, L. M.; Record, M. T. *J. Phys. Chem. B* **2008**, *112*, 9428.

(37) Makhatadze, G. I.; Clore, G. M.; Gronenborn, A. M. *Nat. Struct. Biol.* **1995**, *2*, 852; Antonino, L. C.; Kautz, R. A.; Nakano, T.; Fox, R. O.; Fink, A. L. *Proc. Natl. Acad. Sci. U.S.A.* **1991**, *88*, 7715; Huyghues-Despointes, B. M. P.; Scholtz, J. M.; Pace, C. N. *Nat. Struct. Bio.* **1999**, *6*, 910; Kuhlman, B.; Raleigh, D. P. *Pro. Sci.* **1998**, *7*, 2405.

(38) Parker, M. J.; Clarke, A. R. *Biochemistry* **1997**, *36*, 5786; Shi, Z. S.; Krantz, B.A.; Kallenbach, N.; Sosnick, T. R. *Biochemistry* **2002**, *41*, 2120.

(39) Baghurst, P. A.; Sawyer, W. H.; Nichol, L. W. *J. Biol. Chem.* **1972**, *247*, 3198; Efimova, Y. M.; Haemers, S.; Wierczinski, B.; Norde, W.; van Well, A. A. *Biopolymers* **2007**, *85*, 264; Hattori, A.; Crespi, H. L.; Katz, J. J. *Biochemistry* **1965**, *4*, 1213; Henderson, R. F.; Henderson, T. R.; Woodfin, B. M. *J. Biol.*

Chem. **1970**, *245*, 3733; Kresheck, G. C.; Schneide, H,; Scheraga, H. A. *J. Phys. Chem.* **1965**, *69*, 3132; Masson, P.; Laurentie, M. *Biochim. Biophys. Acta* **1988**, *957*, 111.

(40) Sulistijo, E. S.; MacKenzie, K. R. *J. Mol. Biol.* **2006**, *364*, 974.

(41) Urry, D. W. *J. Phys.Chem. B* **1997**, *101*, 11007.

(42) Cho, Y. H.; Zhang, Y. J.; Christensen, T.; Sagle, L. B.; Chilkoti, A.; Cremer, P. S. *J. Phys.Chem. B* **2008**, *112*, 13765.

(43) Yao, X. L.; Hong, M. *J. Am. Chem. Soc.* **2004**, *126*, 4199.

(44) Nuhn, H.; Klok, H. A. *Biomacromolecules* **2008**, *9*, 2755.

(45) Mao, H. B.; Yang, T. L.; Cremer, P. S. *J. Am. Chem. Soc.* **2002**, *124*, 4432.

(46) Myers, J. K.; Pace, C. N.; Scholtz, J. M. *Pro. Sci.* **1998**, *7*, 383.

(47) Kujawa, P.; Winnik, F. M. *Macromolecules* **2001**, *34*, 4130.

(48) Baker, E. N.; Hubbard, R. E. *Prog. Biophys. Mol. Biol.* **1984**, *44*, 97; Debelle, L.; Alix, A. J. P.; Jacob, M. P.; Huvenne, J. P.; Berjot, M.; Sombret, B.; Legrand, P. *J. Biol. Chem.* **1995**, *270*, 26099.

(49) Maeda, Y.; Higuchi, T.; Ikeda, I. *Langmuir* **2000**, *16*, 7503.

(50) Serrano, V.; Liu, W.; Franzen, S. *Biophys. J.* **2007**, *93*, 2429.

(51) Li, B.; Alonso, D. O. V.; Bennion, B. J.; Daggett, V. *J. Am. Chem. Soc* **2001**, *123*, 11991.

(52) Laukkanen, A.; Valtola, L.; Winnik, F. M.; Tenhu, H. *Macromolecules* **2004**, *37*, 2268.

(53) Johnson, S. J.; Bayerl, T. M.; McDermott, D. C.; Adam, G. W.; Rennie, A. R.; Thomas, R. K.; Sackmann, E. *Biophysical Journal* **1991**, *59*, 289; Tamm, L. K.; McConnell, H. M. *Biophys. J.* **1985**, *47*, 105.

(54) Yang, T. L.; Baryshnikova, O. K.; Mao, H. B.; Holden, M. A.; Cremer, P. S. *J. Am. Chem. Soc.* **2003**, *125*, 4779.

(55) Albertorio, F.; Diaz, A. J.; Yang, T. L.; Chapa, V. A.; Kataoka, S.; Castellana, E. T.; Cremer, P. S. *Langmuir* **2005**, *21*, 7476.

(56) Yang, T. L.; Jung, S. Y.; Mao, H. B.; Cremer, P. S. *Anal. Chem.* **2001**, *73*, 165.

(57) Shi, J.; Yang, T.; Cremer, P. S. *Anal. Chem.* **2008**, *80*, 6078.

VITA

Name:	Youn Hee Cho
Address:	Department of Chemistry, Texas A&M University, MS 3255 College Station, TX 77843
Email Address:	ycho@mail.chem.tamu.edu
Education:	B.S., Chemistry, State University of New York at Purchase, 2004 Ph.D., Chemistry, Texas A&M University, 2009